AN ABSTRACT OF THE THESIS OF

Joseph Wilfred St.Martin for the degree of Master of Science in the School of Oceanography presented on June 17, 1983

Title: Internal Waves: Towed Observations in the Western North Atlantic

Abstract approved: Redacted for Privacy
Clayton A. Paulson

Observations of internal waves were made with a towed thermistor chain between 10 and 110m depth in the Sargasso Sea and north of the Gulf Stream in a warm core ring. Spectral levels agree with the Garrett-Munk spectrum except that a spectral shoulder was observed in the Sargasso Sea observations at a wavenumber of $2\text{-}3\times10^{-3}$ cpm. This shoulder coincides with a coherence peak found when the vertical separation was less than 40m. This coherence peak differs from the Garrett-Munk model, although coherences at low wavenumbers agree. The spectal shoulder and coherence peak is evidence of dominance by a few low modes.

The spectral levels from the Sargasso Sea and warm core ring agree with observations by Katz and Briscoe (1979) from 350 to 750m depth in the Sargasso Sea and with observations from MILE (Spoering, 1979; Levine et al., 1983a) which were taken in the upper ocean in the NE Pacific. The observations from Bell (1976) taken in the

Sargasso Sea and from JASIN (Levine et al., 1983b) taken west of Scotland exhibit higher spectral levels than our observations.

Internal Waves: Towed Observations in the Western North Atlantic

by

Joseph Wilfred St. Martin

A THESIS

submitted to

Oregon State University

in partial fulfillment of
the requirements for the
degree of

Master of Science

Completed June 17, 1983

Commencement June 1984

APPROVED:

Redacted for Privacy

Professor of Oceanography in charge of major

Redacted for Privacy

Dean of the School of Oceanography

Redacted for Privacy

Dean of Graduate School

Date thesis is presented June 17, 1983

Typed by Joseph W. St. Martin for Joseph W. St. Martin

ACKNOWLEDGEMENT

I wish to thank Dr. Clayton Paulson, my major professor, and Dr. Murray Levine for their guidance and assistance in the developement of my thesis.

I also would like to thank Rick Baumann for his expertise and assistance with the computer and Lynn deWitt for her advice. Most of all, I wish to thank my wife, Debbie, for her support and love. These last few months have been hectic and she has helped me make it from day to day.

This research is supported by the the U. S. Coast Guard which had enough faith in my abilities to assigned me to graduate school and the Office of Naval Research, contract N00014-79-C-0004, project NR 083-102.

TABLE OF CONTENTS

LIST OF FIGURES

LIST OF TABLES

INTERNAL WAVES: TOWED OBSERVATIONS IN THE WESTERN NORTH ATLANTIC

INTRODUCTION

Until recently, upper ocean internal waves were not as extensively studied as those at deeper depths. Roth et al. (1979) compared data from the upper ocean available at that time. Recent additional studies have been published which provide a broader observational base. Summaries of internal wave observation and theory can be found in Munk (1979) and Levine (1983).

Internal waves in the deep ocean, where the buoyancy frequency, N, given by $N = (g/\rho \, \partial\rho/\partial z)^{1/2}$, varies little with depth, have been extensively investigated. Garrett and Munk (1972, 1975, 1979) have modeled the distribution of internal wave energy in this region. The slowly varying buoyancy frequency allowed the use of the WKB approximation in the formulation of the model. This model adequately describes the internal wave spectra at frequencies greater than the inertial frequency and less than the local buoyancy frequency. However, the Garrett-Munk model may not be applicable in the upper ocean, where the bouyancy frequency changes rapidly and where there may be sources or sinks of internal wave energy.

In the upper ocean, deviations from the Garrett-Munk model have been observed. Pinkel (1975, 1981) found higher levels of spectral energy and a peak in vertical coherence at frequencies of 3 to 6 cph. These deviations were explained as the result of dominance by the lowest few modes. Levine et al. (1983a, 1983b) found similar results at high frequency and wavenumber and successfully modeled the internal wave spectra with a model composed of only the lowest few modes. At 350m depth in the Sargasso Sea, Katz and Briscoe (1979) also observed a peak in the coherence. This was again concluded to be the result of low mode dominance. The reason for low mode dominance has not been explained.

The purpose of this paper is to present the results of observations made with a towed thermistor chain in the western North Atlantic. Data were obtained at depths between 10 and 110m at two separate locations. Horizontal wavenumber spectra and towed vertical coherences at various vertical separations are presented. These results are compared to other observations and to the Garrett-Munk model.

OBSERVATIONS

Observations were made with a towed thermistor chain in September, 1981. A diagram of the thermistor chain is shown on Fig. 1. The chain consisted of a wire strain member wound to a drum and connected to a streamlined, cylindrical, 450kg depressor. Plastic fairings were attached to the strain member throughout its length. Sensors and electronics were incorporated within some of the fairings. These consisted of 31 thermistors, 3 pressure sensors, and 2 conductivity sensors. Analog signals from each of the sensors were sampled at a frequency of 4Hz and recorded on magnetic tape. The system provided a record of temperature, pressure, or conductivity vs. time and distance at the depth of each sensor. Table 1 lists the locations of the sensors on the chain and their mean depth in the water column during the two data collection tows. Spoering (1979) provides a more detailed description of the thermistor chain.

The thermistor chain was towed on three separate occasions during the cruise (hereafter referred to as Runs 1, 2, and 3). Data from Run 1 were not analyzed because the chain was deployed to a depth of only 70m and a variety of water types were crossed. Tow tracks for Runs 2 and 3 are shown in Fig. 2. Run 2 was located in the Sargasso Sea and Run 3 was located north of the Gulf

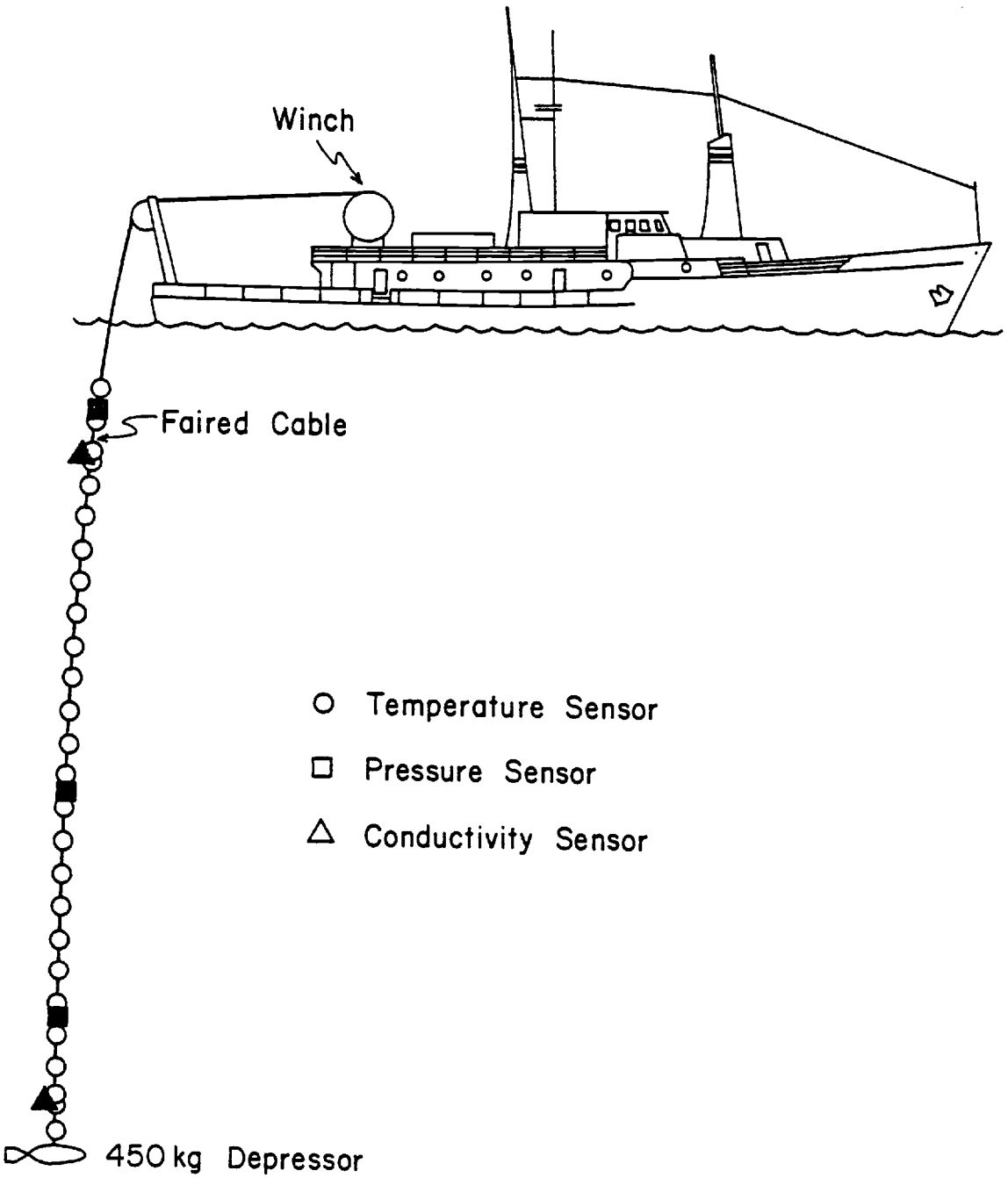

Figure 1. Configuration of the thermistor chain while under tow.

Table 1. Location and mean depth of operating towed chain sensors. Each station has either a temperature (T), pressure (P), or conductivity (C) sensor installed. The distance along the chain from the depressor to the sensors is denoted by S with units of chain-meters. One chain meter equals 1.016 m.

Channel No.	Station	S (Chain-meters)	Depth of Operating Sensors (m) Run 2	Run 3
1	P0	10	116.7	107.2
2	T1	12	114.7	105.2
3	T2	16	110.6	101.1
4	C0	16.5	110.1	100.6
5	T3	17	109.6	100.1
7	T4	20	106.6	97.1
9	T6	28	98.5	89.2
10	T7	32	94.5	85.2
11	T8	36	90.5	81.3
12	T9	40	86.5	77.5
13	T10	44	82.5	73.6
16	T13	56	70.7	62.3
18	T14	60	66.8	58.6
19	T15	64	62.8	55.0
21	T17	72	55.1	47.8
23	T19	80	47.4	40.7
24	T20	84	43.6	37.3
25	T21	88	39.8	33.8
27	T23	96	32.2	27.1
28	T24	100	28.5	23.8
29	T25	104	24.8	20.5
30	P2	106	22.9	18.9
31	T26	108	21.1	17.3
32	T27	112	17.4	14.1
34	C1	116.5	13.3	10.6
35	T29	117	12.8	10.2
36	T30	120	10.1	7.8

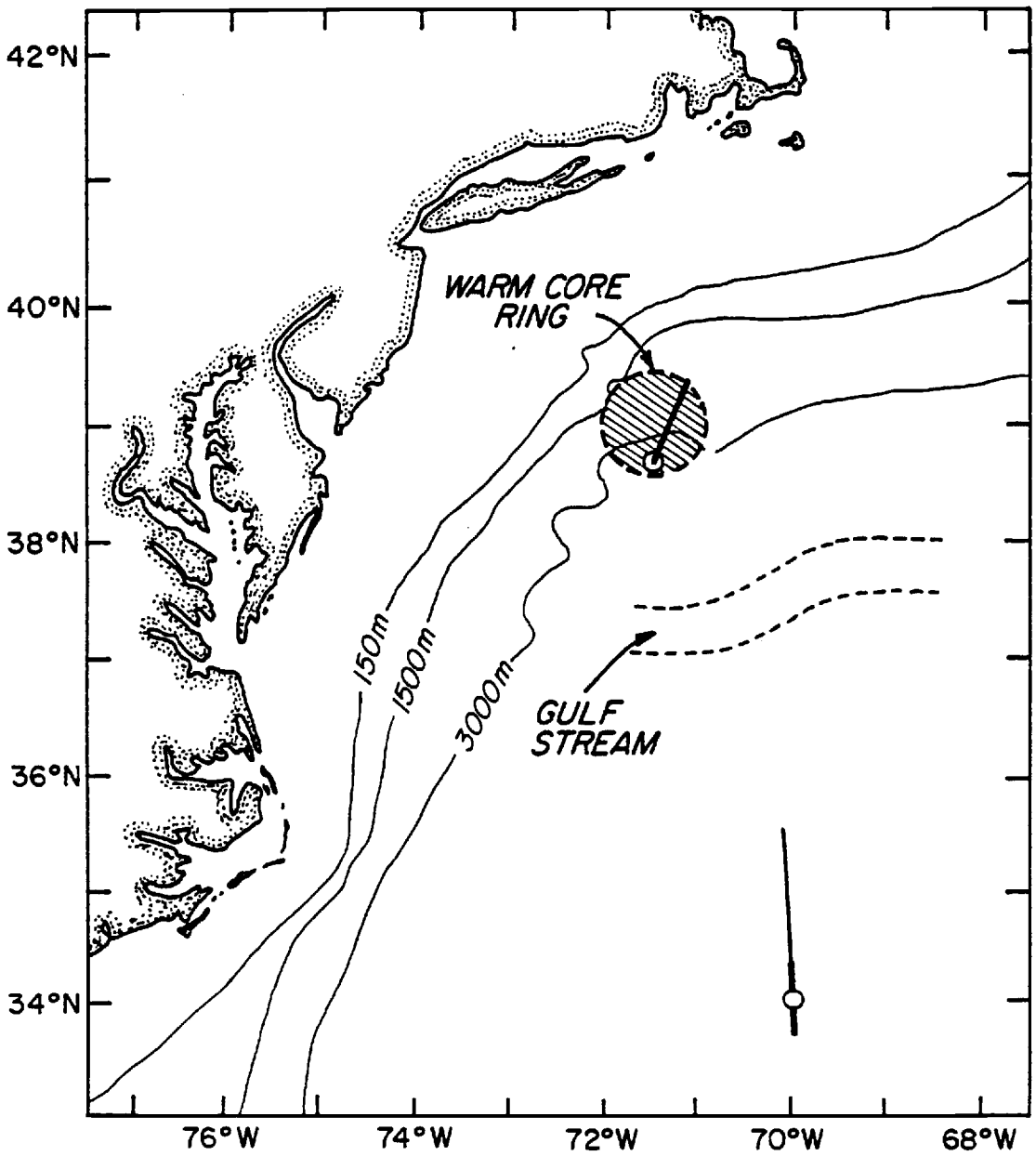

Figure 2. Chart showing the ship's cruise track and approximate location of the Gulf Stream and a warm core ring. The heavy segment in the Sargasso Sea corresponds to Run 2 and the one within the warm core ring is Run 3. The light segment corresponds to an XBT cross-section which extends beyond the tow track of the chain. Positions of CTD's are also plotted as open circles.

Stream in a warm core ring. During each run data were collected on two separate computer tapes, causing a short break in the record. Some of the data were not used because of changes in tow speed or the crossing of water structure not associated with internal waves. Table 2 summarizes observations which were analyzed.

Observations of temperature and conductivity vs. depth (Trask et al., 1982) were taken at two sites near the locations of Runs 2 and 3 (see Fig. 2). The buoyancy frequency, $N = (g/\rho \, \partial\rho/\partial z)^{1/2}$, computed from these observations is shown in Figs. 3 and 4.

Observations of temperature vs. depth were taken at near hourly intervals with expendable bathythermograph (XBT) probes. Appendix A contains vertical temperature profiles and contoured isotherms from XBT casts taken during Runs 2 and 3 and extending beyond Run 2. The locations of the XBT measurements is shown in Fig. 2.

Table 2. Summary of isotherms spectrally analyzed. Isotherms are at 0.5 deg C intervals.

Isotherm (Deg C)	Tape	Begin Time/Date (GMT)	Duration (min)	Tow Speed (m/s)
Run 2				
21 through 25.5	9	0130 14-Sep-81	314	2.0
21 through 25.5	10	0646 14-Sep-81	300	2.0
20 and 20.5	10	0730 14-Sep-81	255	2.0
Run 3				
18 through 22	12	1915 17-Sep-81	282	2.8
20 through 22	13	0057 18-Sep-81	160	2.5

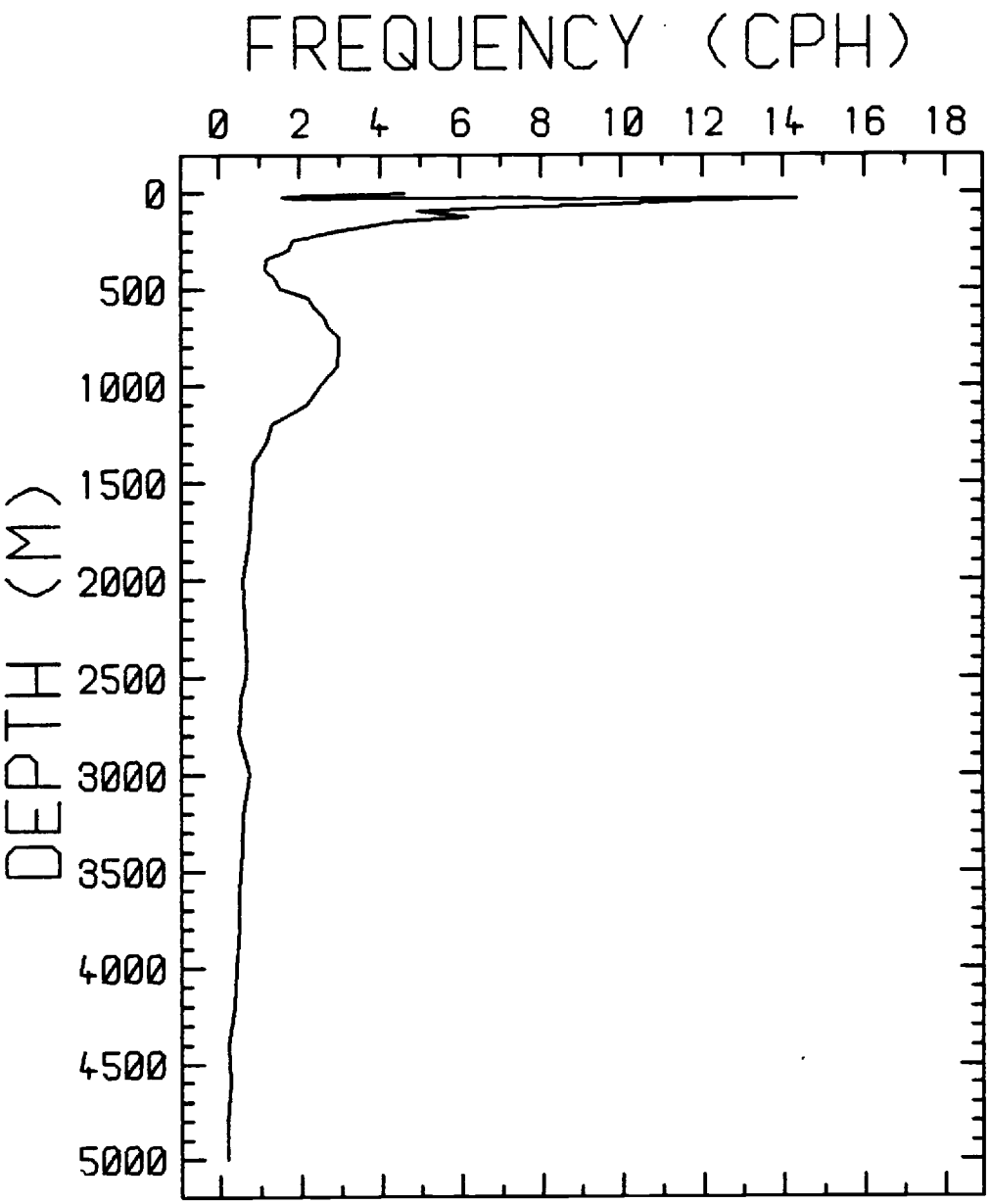

Figure 3. Buoyancy frequency in the Sargasso Sea near Run 2 on 13-Sep-81 (Trask et al., 1982).

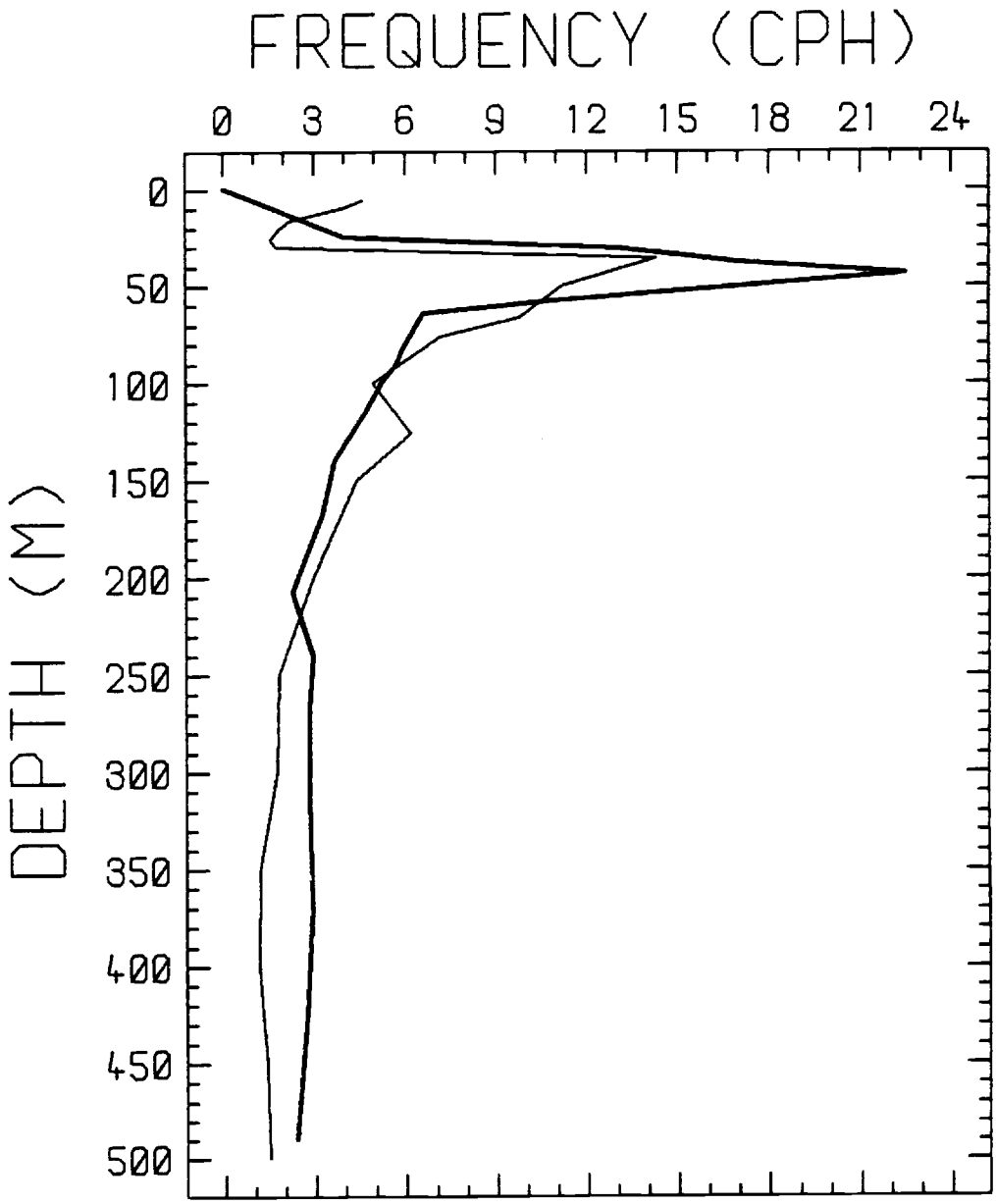

Figure 4. Buoyancy frequency from a warm core ring (Run 3) on 17-Sep-81 (heavy line) and from the Sargasso Sea (Run 2) on 13-Sep-81 (light line) (Trask et al., 1982).

ANALYSIS

The raw temperature, pressure, and conductivity data were low-pass filtered by computing sequential 30s averages. This filtering removed fluctuations in chain depth caused by surface gravity waves and the roll, pitch, and heave of the ship.

The temperature data was used to compute the depths of isotherms (at 0.5 deg C intervals) by linear interpolation between the records. These isotherm depths were edited to remove records which were less than 80% complete due to internal waves with large amplitudes moving out of the limited depth range of the chain. Records which were more than 80% complete were completed by extrapolation from adjacent isotherms. The edited isotherm depths from Runs 2 and 3 are shown in Appendix B.

During Run 3, the chain tended to kite (move to the side) because of the greater tow speed. The 30s averages of pressure provided a record of the vertical movement of the chain caused by the kiting. This pressure record was used to correct the isotherm depths. The correction was performed by linear interpolation between the deep and shallow pressure record. Isotherm depths from Run 3 are less reliable than Run 2 because of uncertainties in the correction. Corrections to Run 2 were negligible.

Spectra of isotherm depths were computed by use of standard techniques. Data were first pre-whitened by taking the first forward difference. Pre-whitening minimizes leakage from band to band (Frankignoul, 1974). Spectra were then computed by use of conventional Fourier Transform techniques. The spectra were recolored by dividing by the transfer function of the differencing scheme.

The spectra were smoothed by averaging in non-overlapping wavenumber bands, equally spaced on a logarithmic scale. Frequency spectra were converted to wavenumber spectra by using Taylor's hypothesis and taking the mean tow speed during each run as the relevant velocity. A representative spectrum is shown in Fig. 5. Spectra of individual isotherm depths were also ensemble averaged with other spectra from similar depths. The average spectra for Runs 2 and 3 are shown in Appendix C. Table 2 lists the isotherms used for spectral analysis and their lengths.

Towed vertical coherence (hereafter referred to as coherence) is a measure of the correlation between isotherms vertically separated in the water column. Coherence was only computed for Run 2 because the kiting of the chain during Run 3 tended to cause erroneous coherence values.

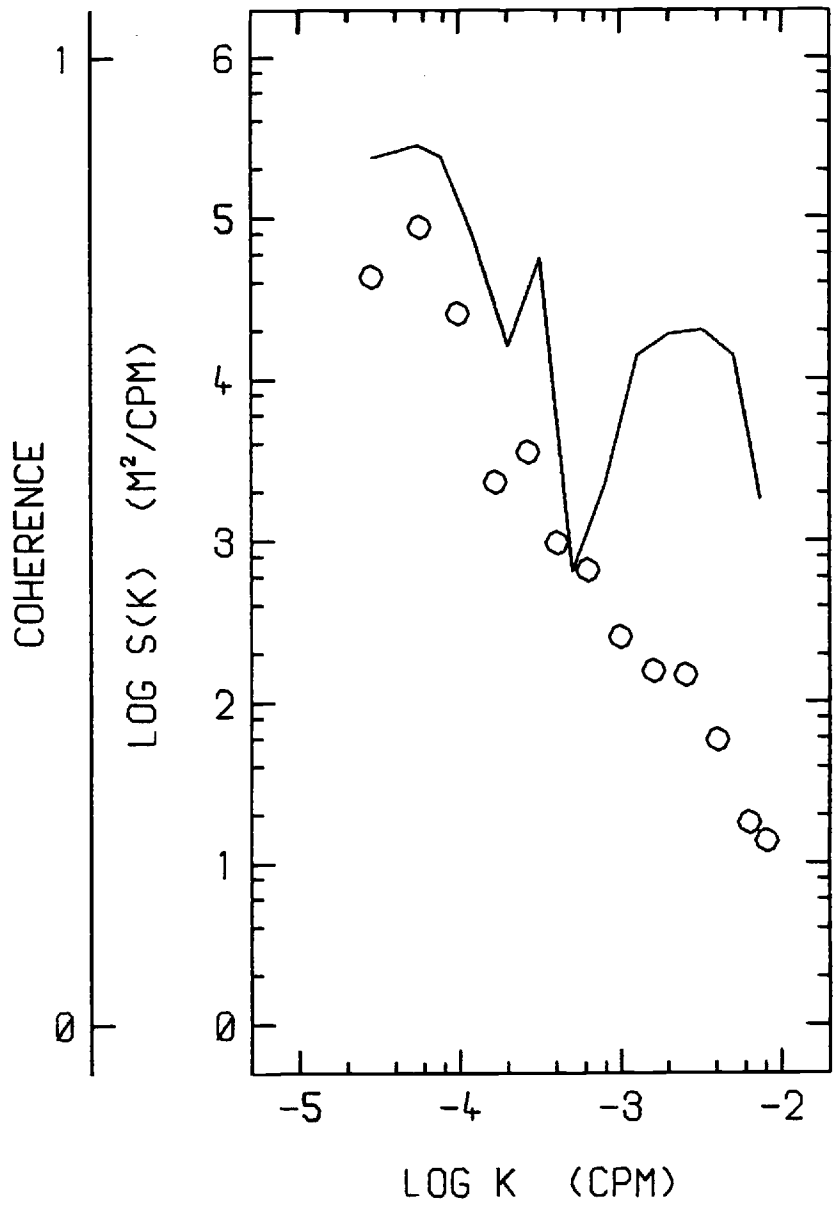

Figure 5. Spectrum of the depth of the 23.5 deg C isotherm (O) from the Sargasso Sea compared to the ensemble averaged coherence with 5 to 10m vertical separation (solid line).

The coherence between isotherm depths is found by computing the cross-spectrum of the two series. This results in a real part, the co-spectrum, and an imaginary part, the quad-spectrum. The coherence squared is given by the ratio of the magnitude of the cross-spectrum to the product of the spectrum of each series. The coherence is the square root of this result. As with the spectra, the cross-spectra are smoothed by averaging over non-overlapping wavenumber bands, equally spaced on a logarithmic scale. Ensemble averaged coherences were computed for isotherm depths of various vertical separations and over all depth levels. A representative coherence spectrum is shown in Fig. 5.

The coherence estimates were tested for significance at the 95% level with the null hypothesis test. Coherence values which fall at or below $(1-.05^{\frac{1}{n-1}})$, where 2n is the degrees of freedom of the estimate, are considered not significantly different from zero at the 95% level.

SPECTRA

Averaged spectra from three depth ranges in the Sargasso Sea are shown in Fig. 6a. The spectral levels increase with increasing depth. When these spectra are scaled by multiplying by the local buoyancy frequency, N(z), as in Fig 6b, the scatter among the spectra is reduced. This suggests that the spectra in the upper 110m of the Sargasso Sea scale with the local buoyancy frequency in agreement with the model of Garrett and Munk (1972, 1975).

These three spectra were multiplied by N and averaged together to create an ensemble averaged spectrum shown in Fig. 7. This spectrum is compared with the spectral model of Garrett and Munk as formulated by Desaubies (1976). The towed spectrum is given by

$$TS(k)=\left(\frac{2}{\pi}\right)^3 \frac{rtf}{N}\int_f^N\int_k^\infty (\omega^2-f^2)^{3/2}\ \omega^3(\rho^2-k^2)^{-1/2}\ \{t^2(\omega^2-f^2)+k^2\}^{-1}\ d\rho d\omega$$

where: $r = Eb^2N_0 = 320\ m^2cph$

$t = j/2bN_0 = 3.8\times10^{-4}$ cpm/cph

$E = 6.3\times10^{-3}$ $\quad j = 3$

$b = 1.3\times10^{3}$ m $\quad N_0 = 3$ cph

The r and t parameters are combinations of the Garrett-Munk parameters: E, the energy level; j, the effective

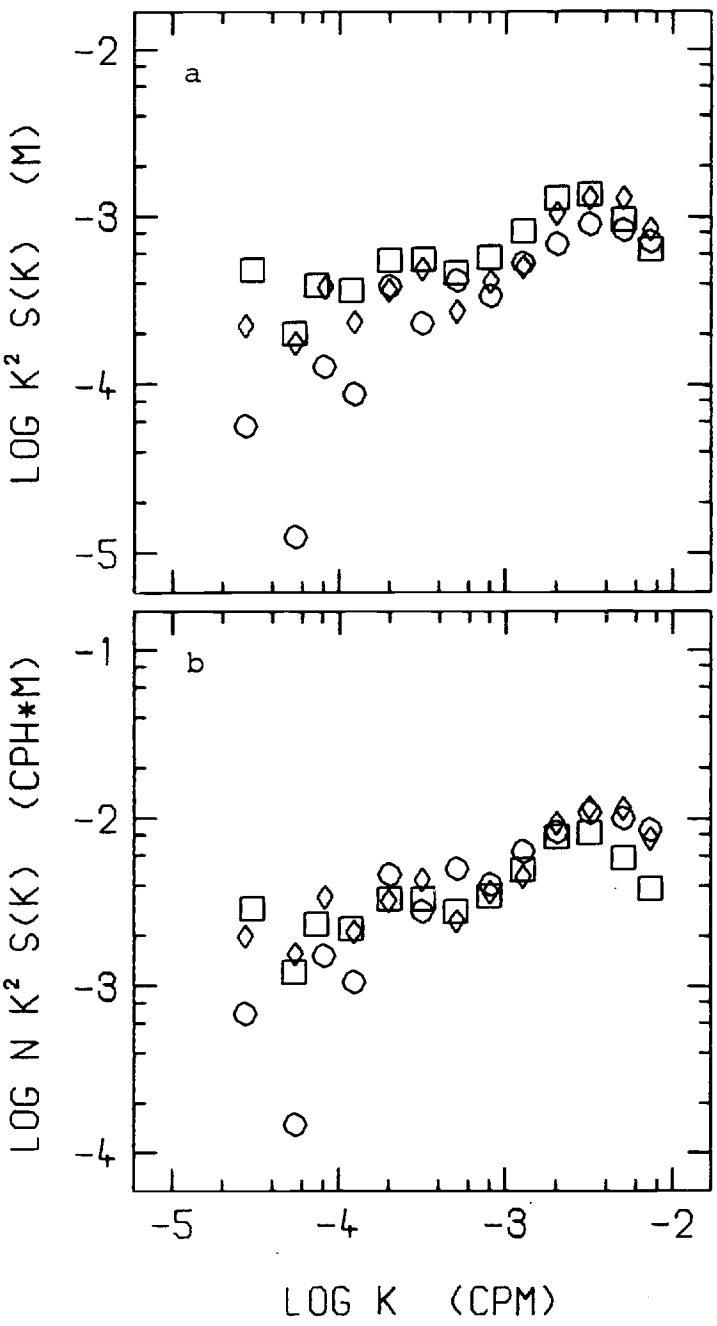

Figure 6. Ensemble averaged spectra of isotherm depth from the Sargasso Sea at depths of 45-50m (○), 76-80m (◇), and 100-110m (□). a) Spectra. b) Spectra scaled by multiplying by the local buoyancy frequency.

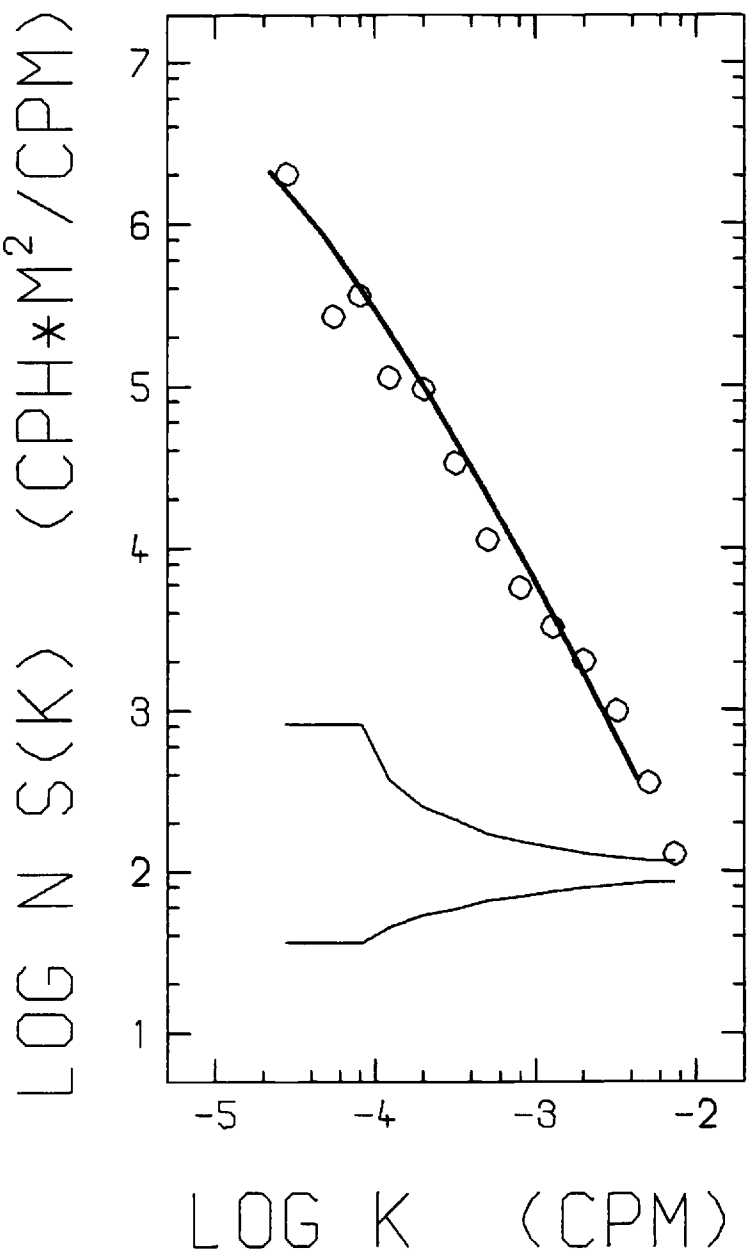

Figure 7. N-scaled average spectrum of isotherm depth from the Sargasso Sea compared to the Garrett-Munk model as formulated by Desaubies (1976). Light lines depict 95% confidence intervals.

mode number; b, the vertical scale of N ; and N_0, the buoyancy frequency scale. This equation was evaluated by numerical integration. At high wavenumbers, the towed spectra has an analytical representation with a k^{-2} slope (Desaubies, 1976).

Overall, the shape and level of the average spectrum agree satisfactorily with the Garrett-Munk model (Fig. 7). However, at wavenumbers lower than $1x10^{-3}$ cpm the spectrum is consistently below the Garrett-Munk model while at higher wavenumbers the spectrum is above the model because of an observed spectral shoulder (flattening of the spectral slope). This spectral shoulder is smeared by the process of averaging individual spectra because the shoulder may not always occur at the same wavelength. The spectral shoulder is more pronounced in some individual spectra as shown in Fig. 5.

Averaged spectra from the warm core ring are shown scaled by the local buoyancy frequency in Fig. 8. These spectra are from depths of 31-35, 35-40, 41-47, and 49-54m with local buoyancy frequencies of 15, 17, 20, and 15 cph respectively. The scaling of these spectra only slightly reduces the scatter of the points. However, there is little variation of buoyancy frequency so that a conclusive statement about N-scaling cannot be made. Fig. 8 also shows the same Garrett-Munk spectral model

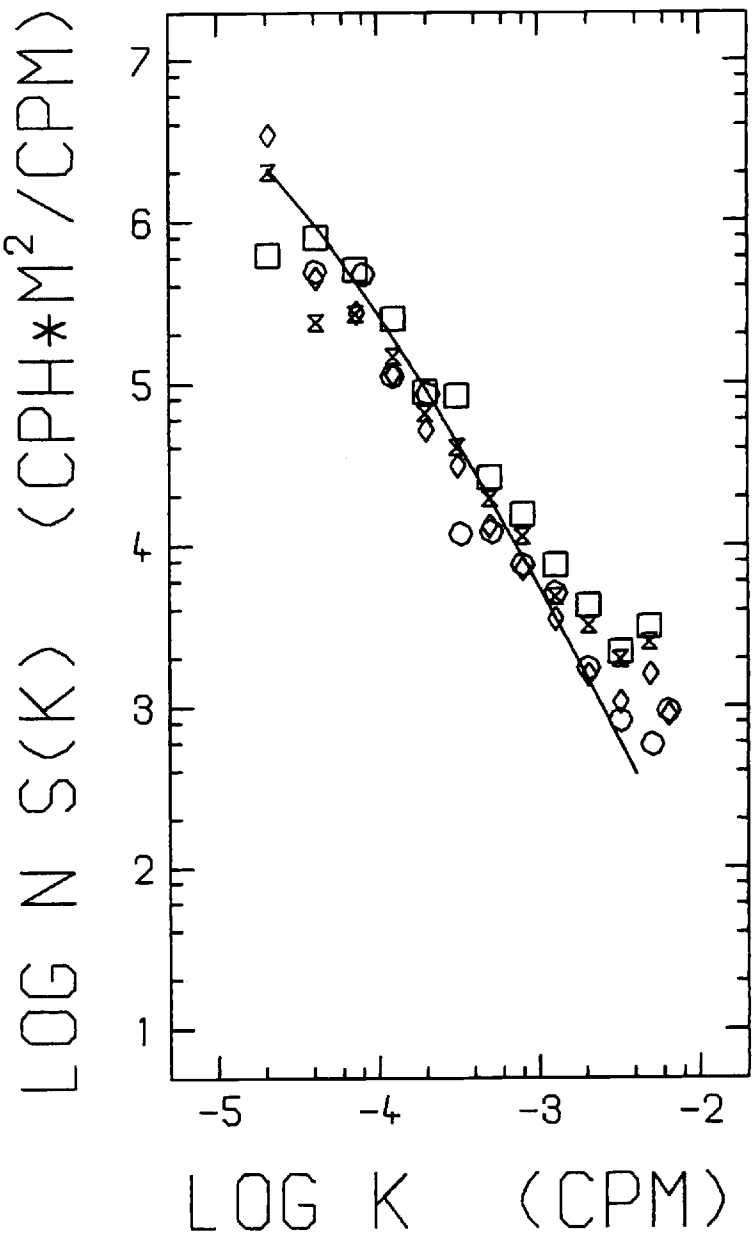

Figure 8. N-scaled ensemble averaged spectra of isotherm depth from the warm core ring at depths of 31-35m (○), 35-40m (◇), 41-47m (⧖), and 49-54m (□) compared to the Garrett-Munk spectral model.

described above. Spectra from the warm core ring agree with the model in level and slope. The increase in observed spectral level at high wavenumbers is fictitious, caused by errors associated with the kiting of the chain. There is no spectral shoulder evident in the spectra.

The averaged spectrum from the Sargasso Sea and the spectrum averaged over 34 to 40m depth from the warm core ring are compared with towed spectra from other experiments and the Garrett-Munk model in Fig. 9. Table 3 summarizes the observations and comparison. The observations from MILE (Spoering, 1979) agree with our results. A spectral shoulder was observed during MILE at a wavenumber of 1×10^{-3} cpm. The deep ocean spectrum of Katz and Briscoe (1979) from a depth of 350 to 750m is also in agreement. This spectrum is the approximate average of spectra which scatter by a factor of ±1.5 around the average. Katz and Briscoe and Spoering concluded that their spectra adequately agreed with the Garrett-Munk model.

In the wavenumber range from 1×10^{-4} to 2×10^{-3} cpm the results from JASIN (Levine et al., 1983b) and Bell (1976) are higher than the others by factors of 2 to 6. The JASIN observations also exhibit a spectral shoulder at a slightly lower wavenumber, 6×10^{-4} cpm. At lower wavenumbers, the spectral levels of the JASIN and Bell

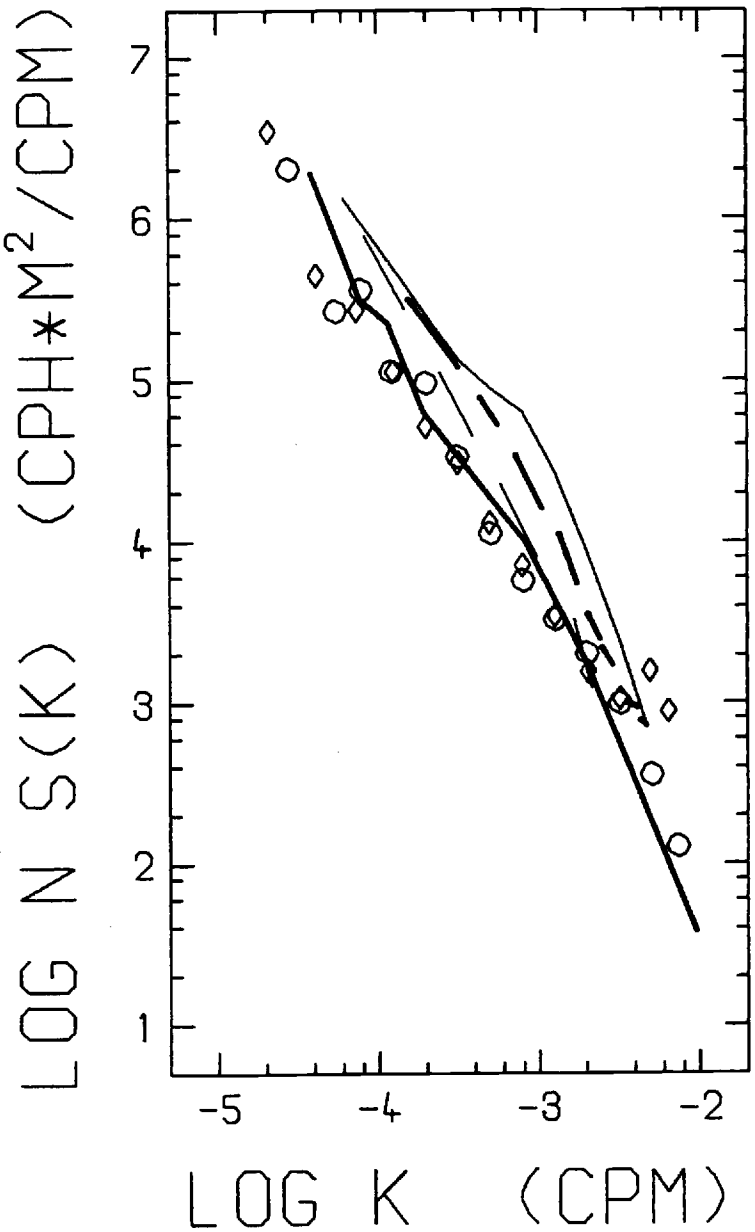

Figure 9. Comparison of N-scaled spectra of isotherm depth from the Sargasso Sea (o), the warm core ring (◊), MILE (heavy solid line), Katz and Briscoe (light dashed line), JASIN (light solid line), and Bell (heavy dashed line).

Table 3. Summary of compared observations of internal waves.

	Run 2	Run 3	Levine et al. (1983a) (MILE)	Levine et al. (1983b) (JASIN)	Bell (1976)	Katz & Briscoe (1979)
Location	Sargasso Sea	Warm core ring	NE Pacific	West of Scotland	Sargasso Sea	Sargasso Sea
Ocean Depth	5000m	2000m	5000m	1500m	1500-5000m	5000m
Observation Depth	45-100m	30-50m	20-40m	20-70m	80-120m	350-750m
Percent Diff. from GM model at $1x10^{-3}$ cpm	+20	+5	+20	+450	+160	+5
Time of Year	Sept	Sept	Sept	Aug	Sept	Oct

observations are more in agreement with the other results and the Garrett-Munk model. This may be due to low statistical significance at low wavenumber.

The coherences from the Sargasso Sea for various vertical separations are compared with the Garrett-Munk model as formulated by Desaubies (1976) (see Appendix D). The values were calculated by numerical integration. A comparison of the observed coherence at 5 to 10m vertical separation with Desaubies' equation using buoyancy frequencies of 6 and 12 cph is shown in Fig. 10. Over the depth range of the data, the mean buoyancy frequency is 9 cph. Therefore the low wavenumber results are consistent with the Garrett-Munk model. Ensemble average coherences for various vertical separations, compared to the Garrett-Munk model, are shown in Appendix E. As the vertical separation increases the number of significant coherence estimates decreases. This makes a comparison to the model more uncertain. However, an overall comparison confirms that the Sargasso Sea results agree with the Garrett-Munk model at low wavenumber.

At high wavenumber, a significant peak in the coherence occurs for vertical separations of less than 40m. This peak does not agree with the Garrett-Munk model which predicts a fall-off to low coherence with increasing

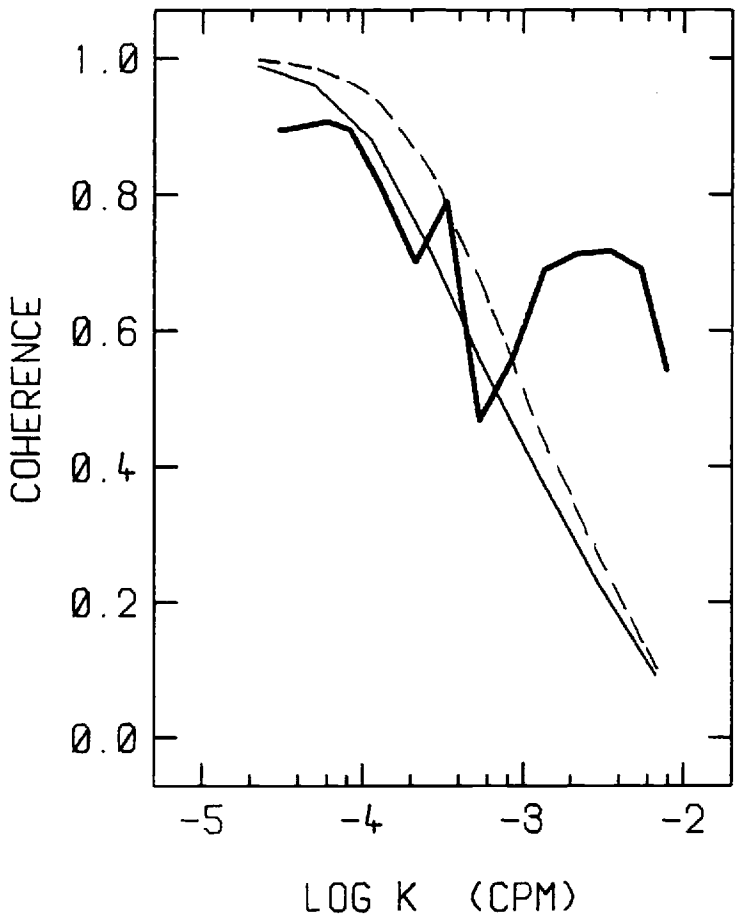

Figure 10. Ensemble averaged coherence between isotherms separated vertically 5 to 10m (bold line) and the Desaubies (1976) towed vertical coherence equation from Appendix D with N = 12 (light line) and N = 6 (dashed line). Desaubies equation computed for a vertical separation of 7.5 m.

wavenumber. This peak is coincident with the shoulders in many of the spectra of individual isotherms (Fig. 5).

Katz and Briscoe (1979) noticed a peak in coherence, at 350m depth, also occurring at $2\text{-}3\text{x}10^{-3}$ cpm. Their observations were made in September in the Sargasso sea approximately 600nm to the east of the site of Run 2. A comparison between the coherence for 5 to 10m vertical separation from Run 2 and the coherence of Katz and Briscoe at 8.5m vertical separation (Fig. 11) shows that their peak, though not as high or broad, occurs at a similar wavenumber. A comparison of the respective buoyancy frequency profiles shows a similar vertical structure with both having a local minimum in the buoyancy frequency at 350m depth. Katz and Briscoe hypothesized that the peak in coherence was due the inabilty of higher modes to "tunnel" into the region of the buoyancy frequency minimum. However, our observations occur in a region of maximum buoyancy frequency. Therefore Katz and Briscoe's explanation does not apply to our data taken at shallow depths.

The coherence peak and spectral shoulder is evidence of dominance of the internal wave spectrum by the lowest few modes at high wavenumber. Pinkel (1975) found that at frequencies from 3 to 6 cph the lowest few modes did dominate. This result is similar to the JASIN (Levine et

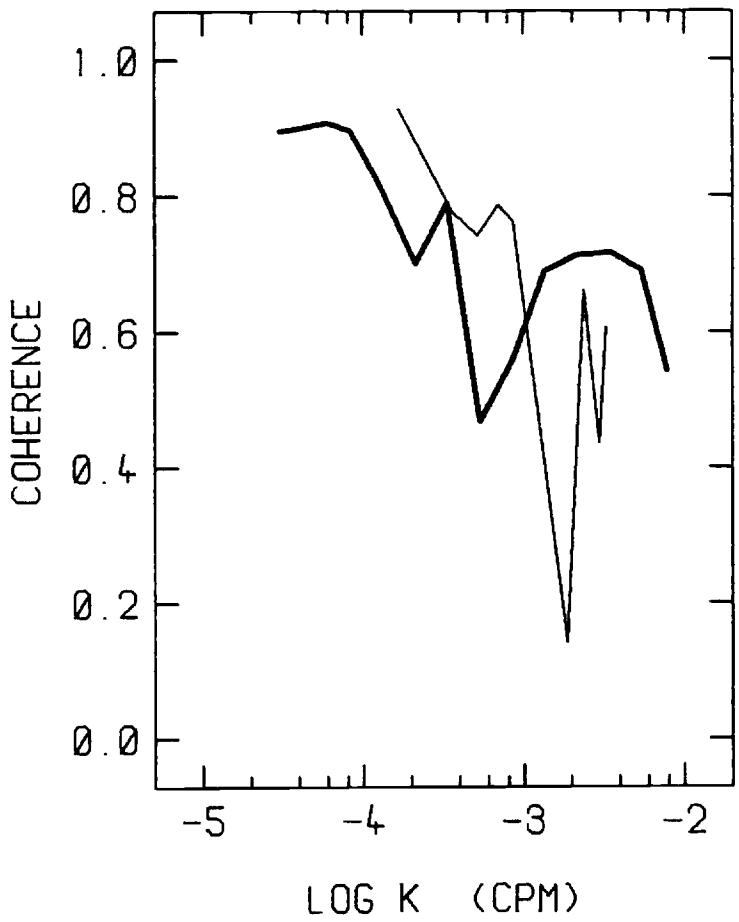

Figure 11. Ensemble averaged coherence between isotherms separated 5 to 10m in the vertical (bold line) and the towed vertical coherence of Katz and Briscoe (1979) at 350m depth and 3.5m vertical separation.

al, 1983b) data previously cited. In frequency space, the JASIN coherence peaked at a frequency of 2 to 4 cph. This corresponded to a wavenumber range of 8×10^{-4} to 2×10^{-3} cpm. The dispersion relation (Fig. 12) for the Sargasso Sea site shows that, at a wavenumber of 2×10^{-3} cpm, the frequency for mode 1 is at least 6 cph and for mode 2 is at least 3 cph. Therefore the internal wave frequencies for the lowest few modes in the wavenumber range of our coherence peak and spectral shoulder correspond to the high frequencies of Pinkel (1975) and JASIN (Levine et al., 1983b). This suggests that the coherence peak found in the Sargasso Sea is due to dominance by the lowest few modes.

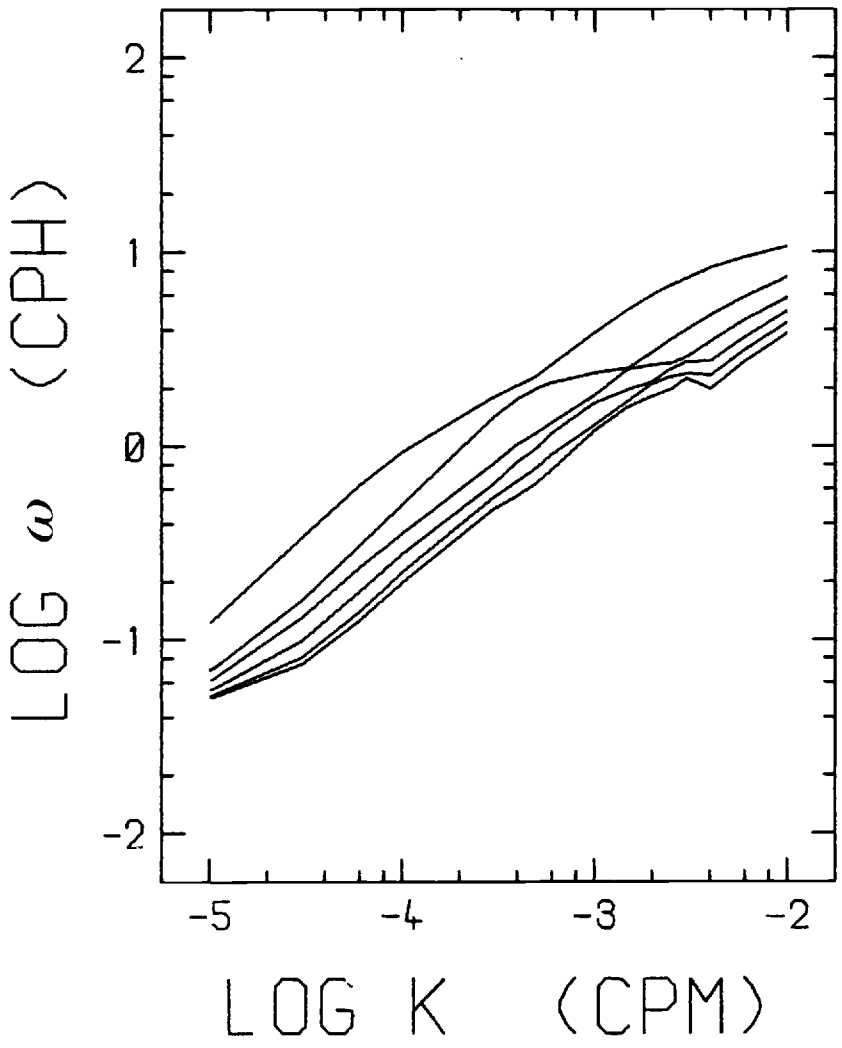

Figure 12. Dispersion relation for modes 1 through 6 in the Sargasso Sea.

CONCLUSIONS

Observations of upper ocean internal gravity waves were made with a towed thermistor chain in September, 1981 at two sites in the western North Atlantic. One site was in the Sargasso Sea and the other was within a warm core ring located north of the Gulf Stream. Spectra of isotherm depths were computed and compared to the predictions of the Garrett-Munk model and to other experiments. The following conclusions can be drawn.

1. The spectral slopes and levels from the Sargasso Sea and the warm core ring agree with the Garrett-Munk model. Averaged spectral levels from the Sargasso Sea are proportional to the local buoyancy frequency.

2. There is a spectral shoulder in the Sargasso Sea results at a wavenumber of $1\text{-}2\times10^{-3}$ cpm. Also at this wavenumber, there is a peak in coherence between isotherms whose vertical separations are less than 40m. This feature does not agree with the Garrett-Munk model. The dispersion relation shows that these wavenumbers correspond to frequencies of at least 3 to 6 cph. The coherence peak and spectral shoulder observed in the Sargasso Sea are evidence of dominance of a few low modes.

3. A comparison of the Sargasso Sea and warm core ring observations was made with other observations in the Sargasso Sea. The results of Katz and Briscoe (1979), taken from 350-750m depth, agree with our results. A peak in coherence was found by Katz and Briscoe at 350m depth whose wavenumber corresponded to our coherence peak. However, the observations of Bell (1976) taken in the upper ocean were generally higher in level by a factor of 2. Bell did not observe a coherence peak or shoulder.

4. A comparison of the Sargasso Sea and warm core ring results was made with experiments conducted in other oceans. The MILE data from the NE Pacific (Spoering, 1979; Levine et al., 1983a) agreed with our results. A spectral shoulder was observed in the MILE towed spectra at $1x10^{-3}$ cpm. The JASIN observations (Levine et al., 1983b) west of Scotland exhibited spectral levels higher than ours by a factor of about 6. A spectral shoulder and coherence peak were observed at $6x10^{-4}$ cpm.

REFERENCES

Baumann, R. J., L. M. deWitt, M. D. Levine, C. A. Paulson, and J. D. Wagner, 1982: Towed Thermistor Chain Observations Across the Gulf Stream. Report, Reference 82-3, School of Oceanography, Corvallis, OR 97331, 98 pp.

Bell, T.H., Jr., 1976: The Structure of Internal Wave Spectra as Determined from Thermistor Chain Measurements. J. Geophys. Res., 81, 3709-3714.

Desaubies, Y. J. F., 1976: Analytical Representation of Internal Wave Spectra. J. Phys. Oceanogr., 6, 976-981.

Frankignoul, C., 1974: A Cautionary Note on the Spectral Analysis of Short Internal Wave Records. J. Geophys. Res., 79, 3459-3462.

Garrett, C. and W. Munk, 1972: Space-Time Scales of Internal Waves. Geophys. Fluid Dynamics, 2, 225-264.

Garrett, C. and W. Munk, 1975: Space-Time Scales of Internal Waves: A Progress Report. J. Geophys. Res., 80,291-297.

Garrett, C. and W. Munk, 1979: Internal Waves in the Ocean. Ann. Rev. Fluid Mech., 11, 339-369.

Gradshteyn, I. S. and I. M. Ryshik, 1965: Tables of Integrals Series and Products. Academic Press, 1086 pp.

Katz, E. J. and M. G. Briscoe, 1979: Vertical Coherence of the Internal Wavefield from Towed Sensors. J. Phys. Oceanogr., 9, 518-530.

Levine, M.D., R.A. de Szoeke, and P.P. Niiler, 1983a: Internal Waves in the Upper Ocean During MILE. J. Phys. Oceanogr., 13, 240-257.

Levine, M.D., C.A. Paulson, M.G. Briscoe, R.A. Weller, and H. Peters, 1983b: Internal Waves in JASIN. Phil. Trans. R. Soc. Lond., 308, 389-405.

Levine, M.D., in press: Internal Waves in the Ocean: A Review. Revs Geophys Space Phys.

Munk, W., 1981: Internal Waves and Small Scale Processes, In: Evolution of Physical Oceanography. Warren & Wunsch, editors, Mit Press, 623 pp.

Pinkel, R., 1975: Upper Ocean Internal Wave Observations from FLIP. J. Geophys. Res., 80, 3892-3910.

Pinkel, R., 1981: Observations of the Near-Surface Internal Wavefield. J. Phys. Oceanogr., 11, 1248-1257.

Roth, M.W., M.G. Briscoe, and C.H. McComas III, 1981: Internal Waves in the Upper Ocean. J. Phys. Oceanogr., 11, 1234-1247.

Spoering, T. J., 1979: Towed Observations of Internal Waves in the Upper Ocean. Report, Reference 79-10, School of Oceanography, Corvallis, OR 97331, 121pp.

Trask, R. P., M. G. Briscoe and N. J. Pennington, 1982: Long Term Upper Ocean Study (LOTUS), A Summary of the Historical Data and Engineering Test Data. Technical Report, WHOI-82-53, Woods Hole Oceanographic Institute, Woods Hole MA, 02534, 107 pp.

APPENDICES

APPENDIX A

XBT Temperature Profiles and Isotherms

This section contains the vertical temperature profiles of XBT data simultaneous to Runs 2 and 3 and extending beyond Run 2. Also shown are contoured isotherms computed by linear interpolation between the XBT temperature data. The offset of the XBT temperature profiles are proportional to the time elapsed between casts. A table listing the position and time of each XBT cast is first.

XBT Drop Sites/Times

Sargasso Sea 14,15-Sep-81

XBT	Position		Time (GMT)
65	33 45.5N	69 59.7W	0100
66	33 47.7N	69 59.9W	0200
67	33 51.3N	69 59.8W	0259
68	33 55.0N	69 59.9W	0400
69	33 58.6N	70 00.3W	0459
70	34 02.3N	70 00.8W	0559
71	34 06.1N	70 01.1W	0659
72	34 10.1N	70 00.9W	0800
73	34 14.1N	70 00.9W	0901
74	34 18.1N	70 00.9W	0959
75	34 22.0N	70 00.7W	1058
76	34 25.7N	70 00.8W	1158
77	34 28.1N	70 00.1W	1610
78	34 38.5N	70 00.0W	1700
79	34 51.6N	69 59.9W	1800
80	35 00.0N	70 00.1W	1843
81	35 03.7N	69 57.6W	2200
82	35 16.0N	69 59.4W	2300
83	35 26.0N	70 00.0W	2357
84	35 37.9N	70 01.8W	0057

Warm Core Ring 17,18-Sep-81

XBT	Position		Time (GMT)
103	38 39.0N	71 29.5W	1830
104	38 42.5N	71 28.8W	1945
105	38 46.1N	71 26.9W	2030
106	38 49.8N	71 25.1W	2115
107	38 53.5N	71 23.2W	2159
108	38 57.5N	71 21.5W	2245
109	39 01.4N	71 19.5W	2330
110	39 05.3N	71 17.4W	0015
111	39 08.9N	71 15.3W	0059
112	39 12.5N	71 13.7W	0145
113	39 16.1N	71 12.2W	0230
114	39 17.9N	71 11.5W	0255
115	39 20.5N	71 10.6W	0330
116	39 21.9N	71 10.0W	0352

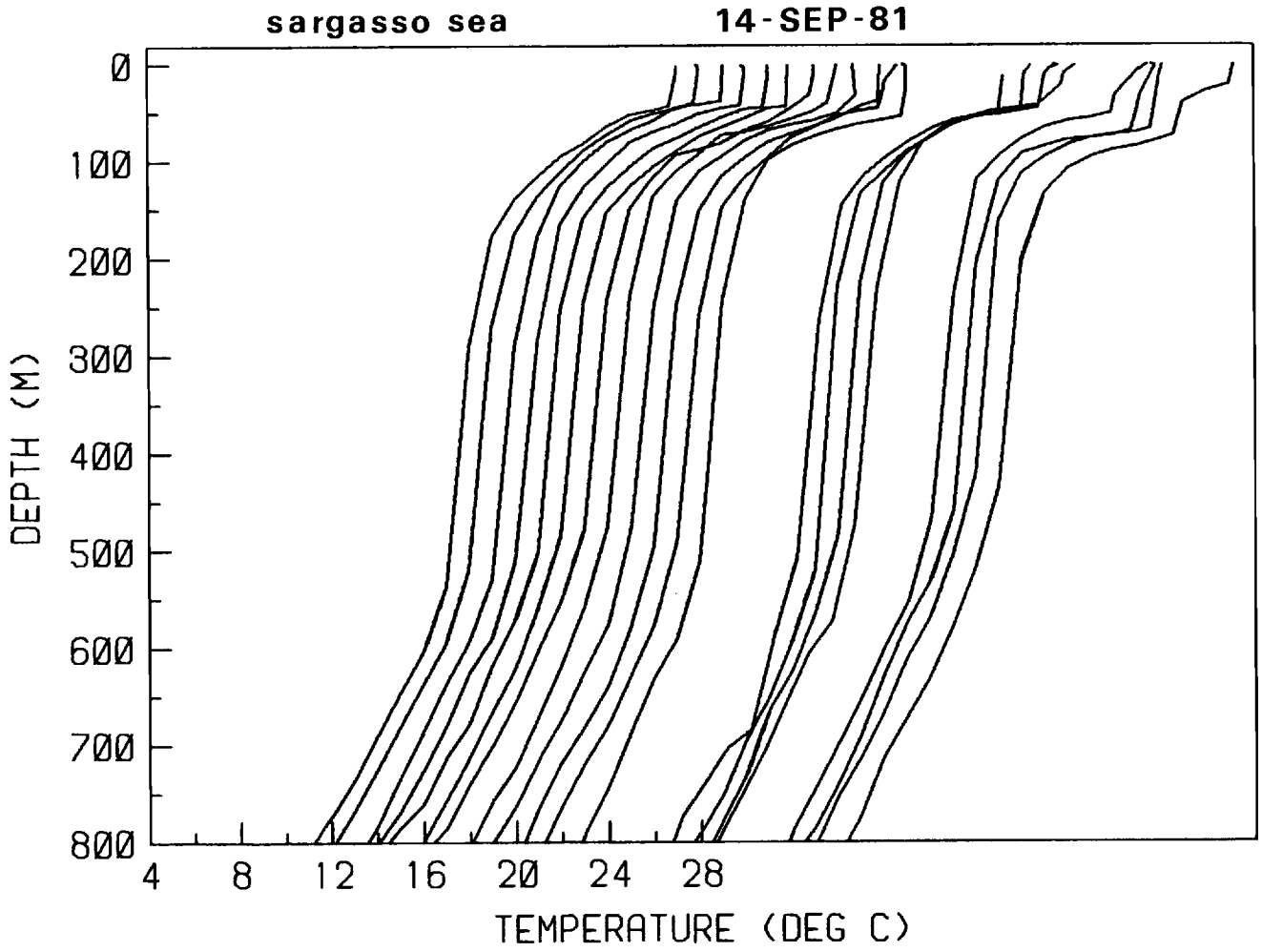
sargasso sea
14-SEP-81
DEPTH (M)
0
100
200
300
400
500
600
700
800
4
8
12
16
20
24
28
TEMPERATURE (DEG C)

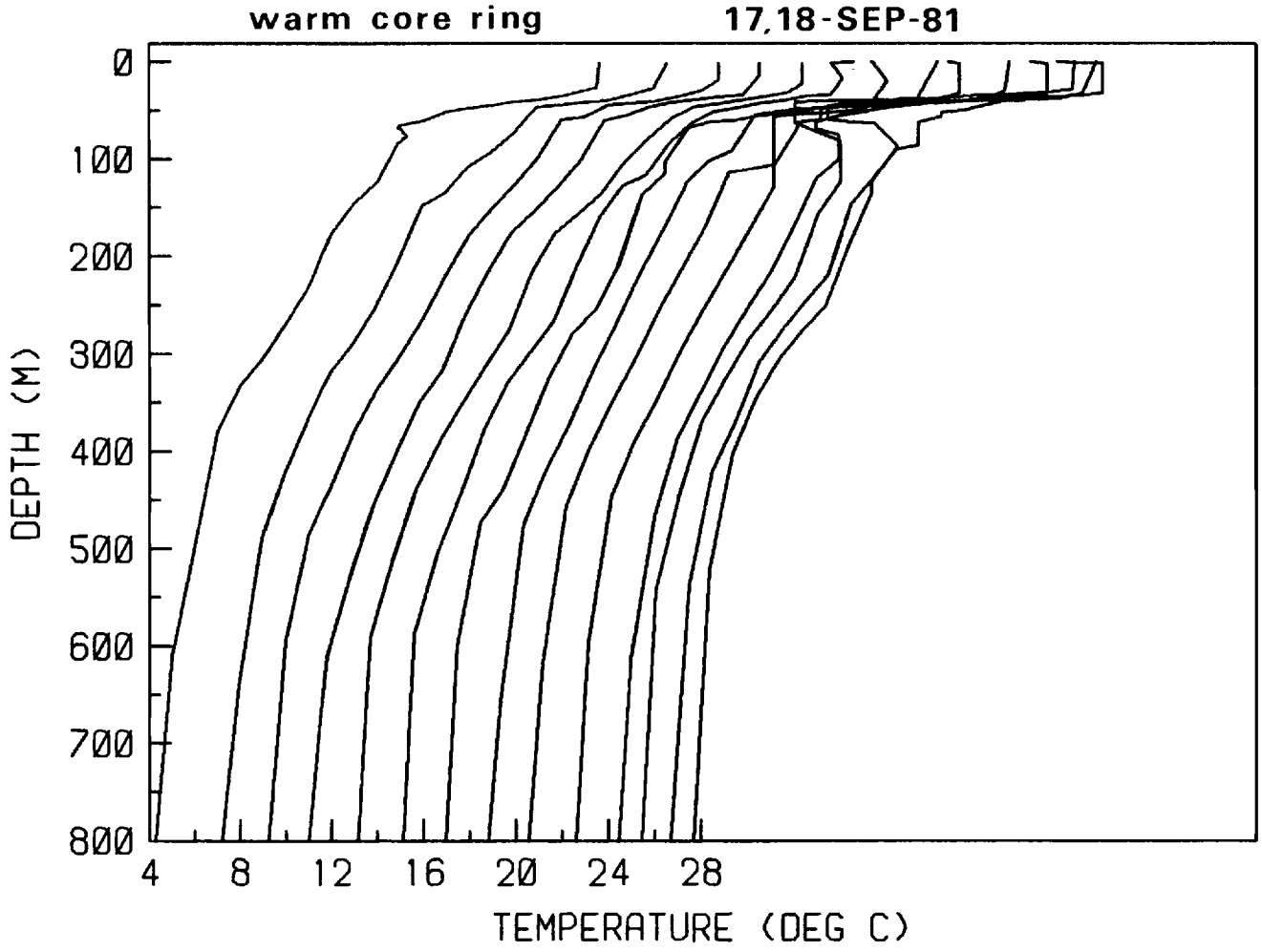
warm core ring
17,18-SEP-81
0
100
200
300
400
500
600
700
800
DEPTH (M)
4
8
12
16
20
24
28
TEMPERATURE (DEG C)

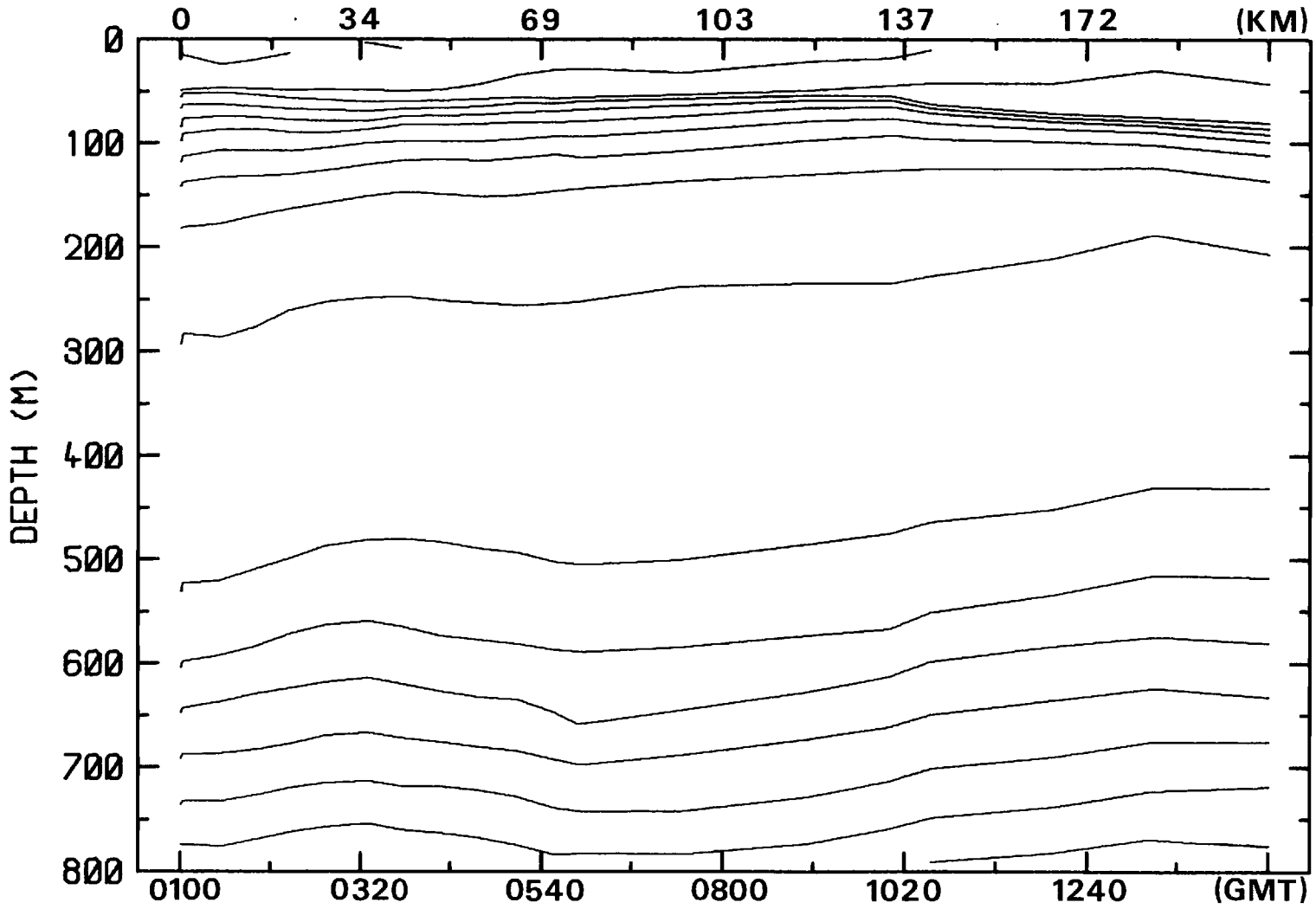

XBT ISOTHERMS VS TIME/DISTANCE 14-SEP-81

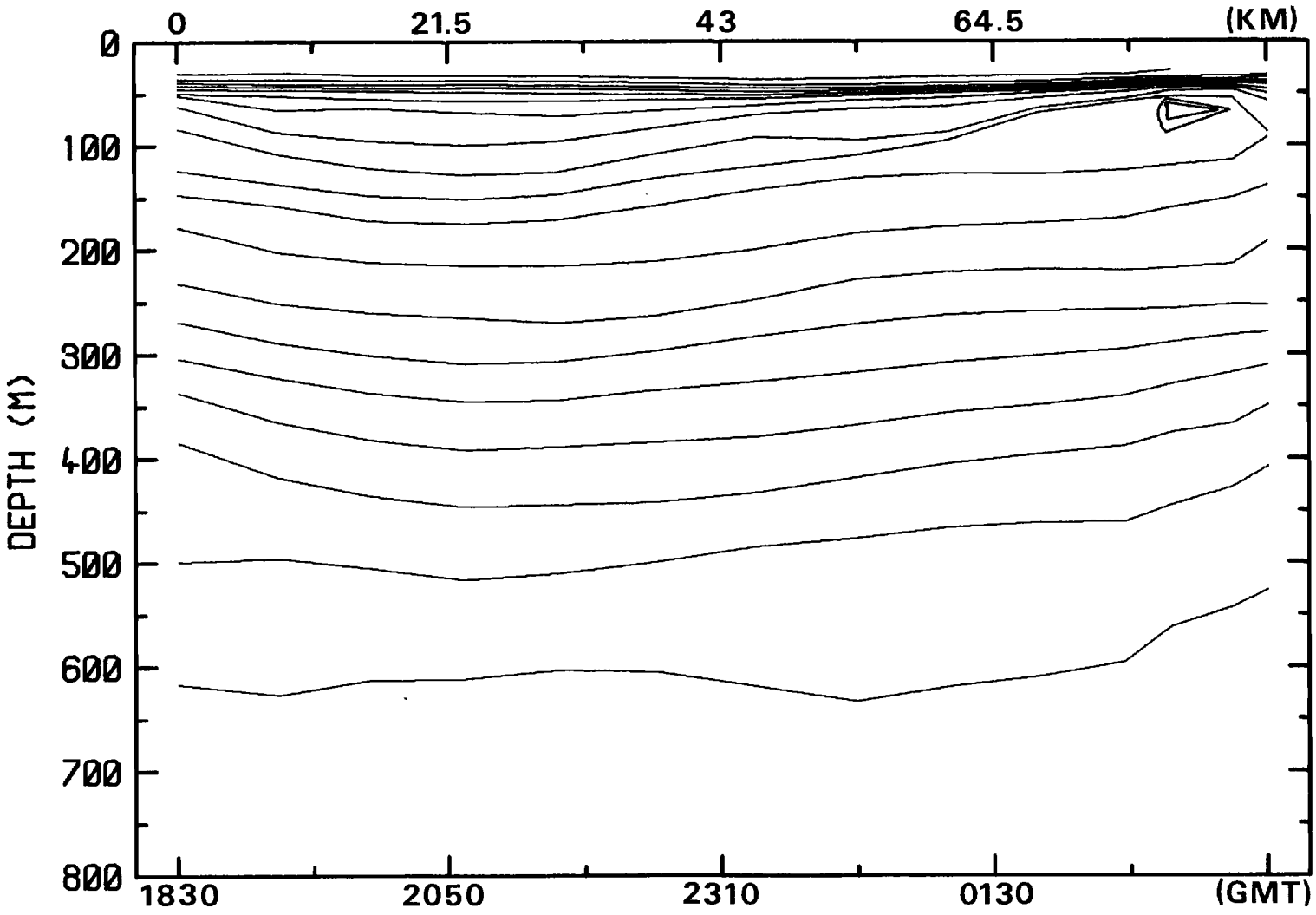

XBT ISOTHERMS VS TIME/DISTANCE 17,18-SEP-81

APPENDIX B

Edited Isotherms

This appendix contains edited isotherm depths from Runs 2 and 3 which were spectrally analyzed. The isotherms and the times at which they were observed are listed first. The highest and lowest isotherm are given on each figure. Intermediate isotherms are at increments of 0.5 deg C.

Isotherms Used for Spectral Analysis

Run 2 14-Sep-81

Isotherm (Deg C)	Time (GMT)	Average Depth (M)
	Tape 9 14-Sep-81	
21.0	0130-0644	104.87
21.5	"	93.78
22.0	"	84.31
22.5	"	76.62
23.0	"	70.03
23.5	"	64.25
24.0	"	58.95
24.5	"	54.08
25.0	"	49.43
25.5	"	45.60
	Tape 10 14-Sep-81	
21.0	0646-1145	90.80
21.5	"	83.12
22.0	"	76.15
22.5	"	70.10
23.0	"	65.37
23.5	"	61.53
24.0	"	57.95
24.5	"	54.69
25.0	"	51.46
25.5	"	48.00
20.0	0730-1145	110.57
20.5	"	99.72
	Tape 12 17-Sep-81	
18.0	1915-2357	53.27
18.5	"	49.51
19.0	"	46.88
19.5	"	44.77
20.0	"	43.00
20.5	"	41.36
21.0	"	39.73
21.5	"	37.97
22.0	"	36.17
	Tape 13 18-Sep-81	
20.0	0057-0337	35.76
20.5	"	34.96
21.0	"	34.09
21.5	"	33.07
22.0	"	31.82

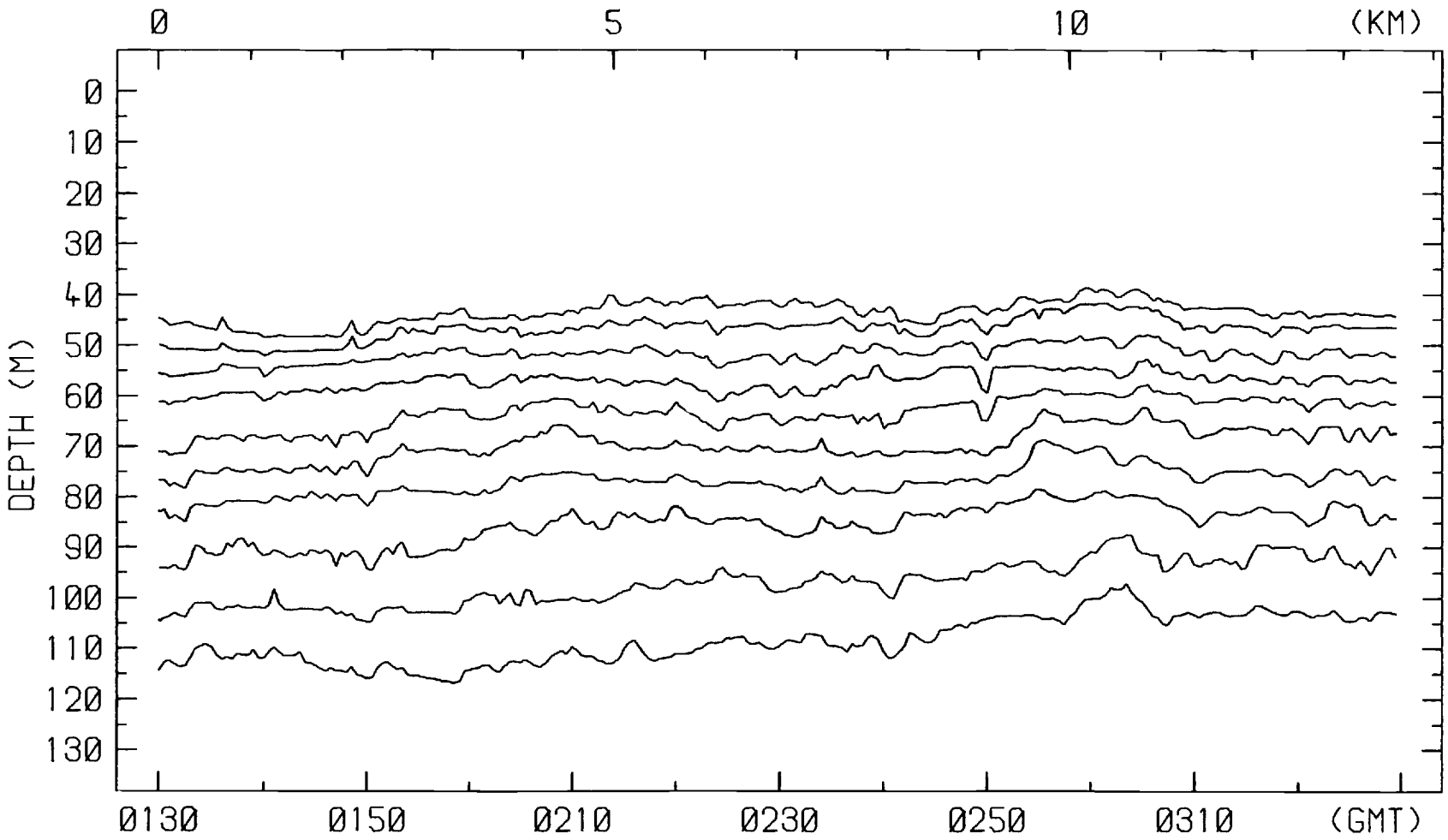

EDITED ISOTHERM DEPTH VS TIME/DISTANCE 14-SEP-81
ISOTHERMS 25.5 TO 21.0 DEG C

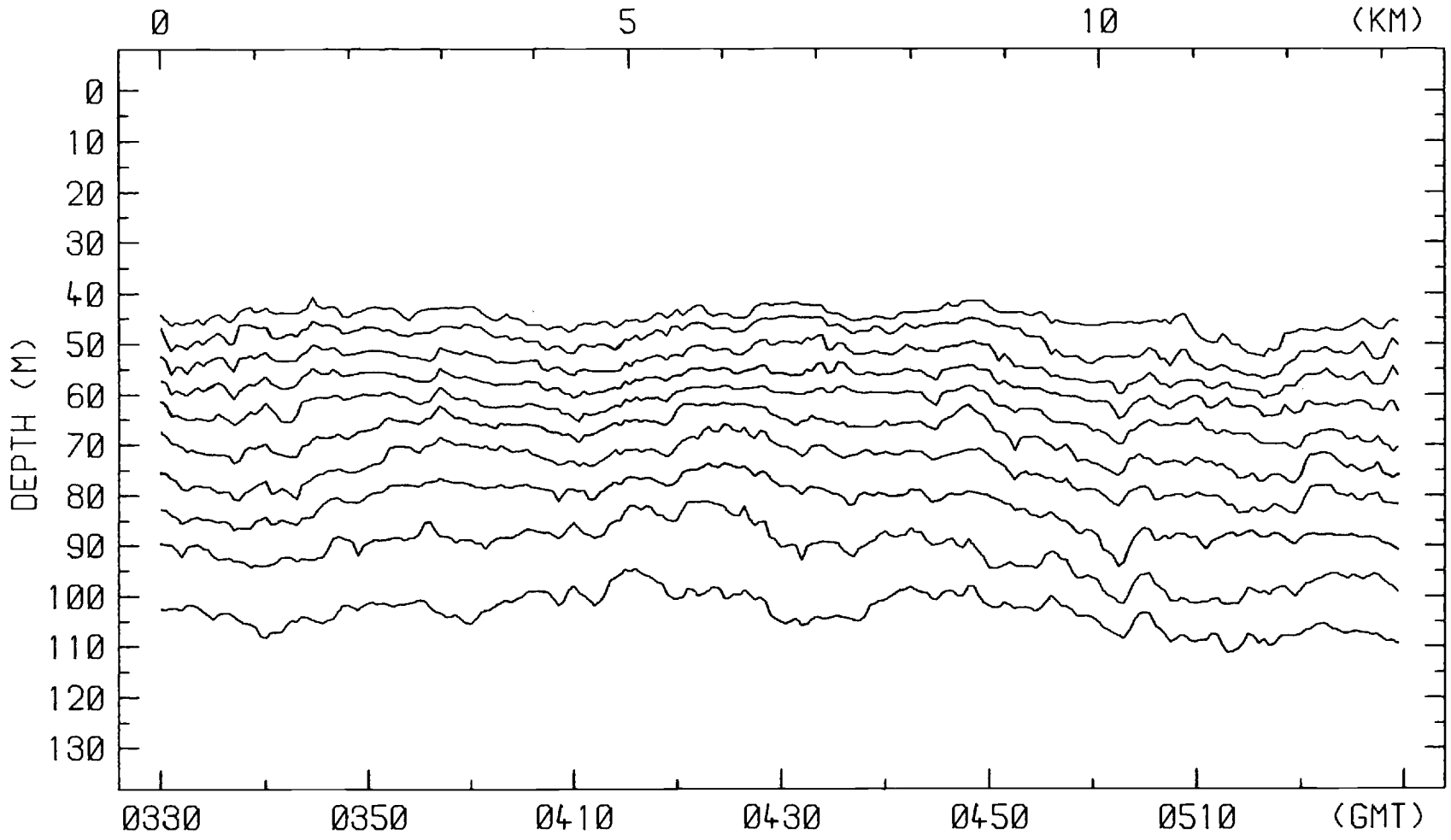

EDITED ISOTHERM DEPTH VS TIME/DISTANCE 14-SEP-81
ISOTHERMS 25.5 TO 21.0 DEG C

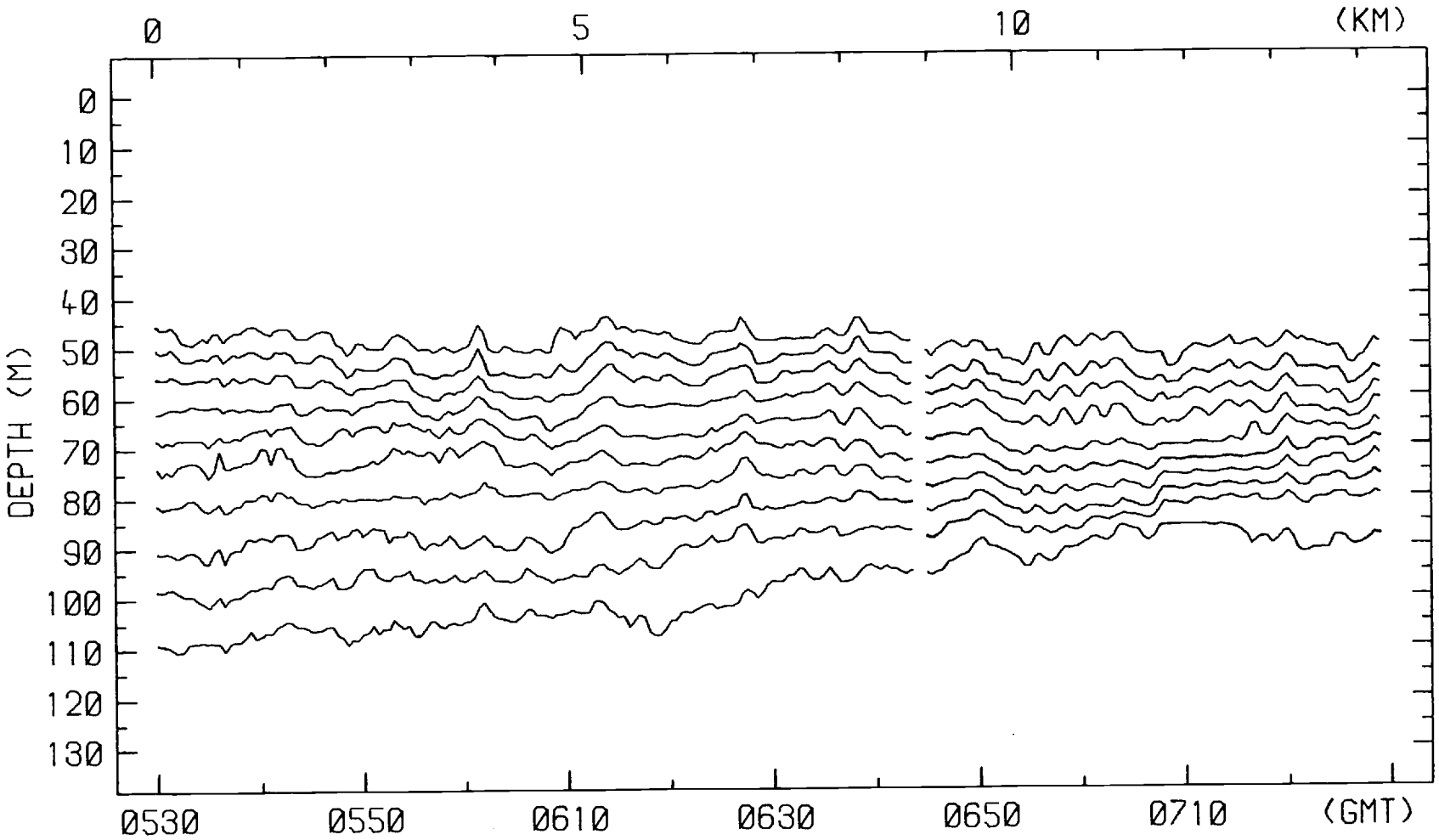

EDITED ISOTHERM DEPTH VS TIME/DISTANCE 14-SEP-81
ISOTHERMS 25.5 TO 21.0 DEG C

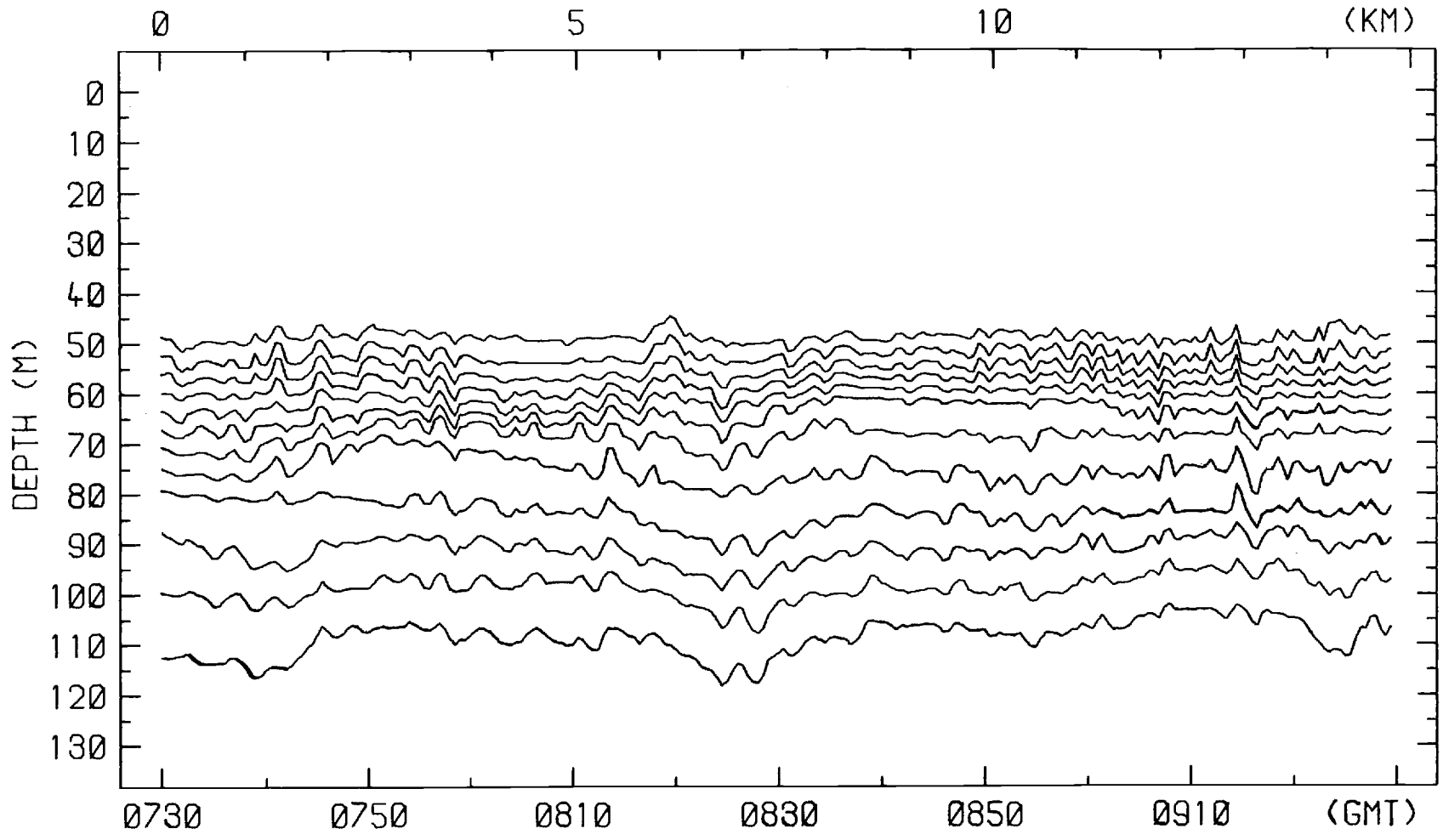

EDITED ISOTHERM DEPTH VS TIME/DISTANCE 14-SEP-81
ISOTHERMS 25.5 TO 20.0 DEG C

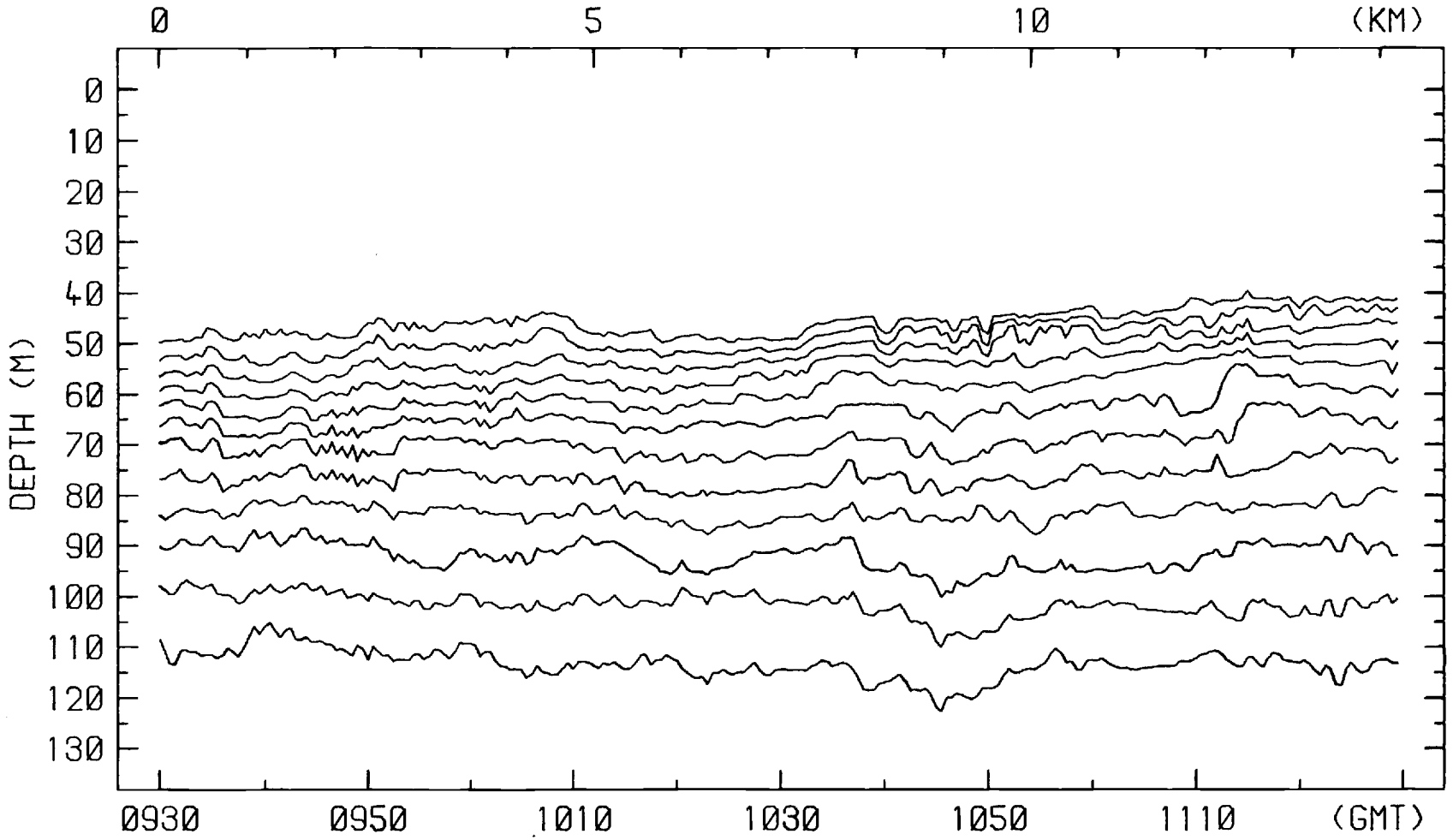

EDITED ISOTHERM DEPTH VS TIME/DISTANCE 14-SEP-81
ISOTHERMS 25.5 TO 20.0 DEG C

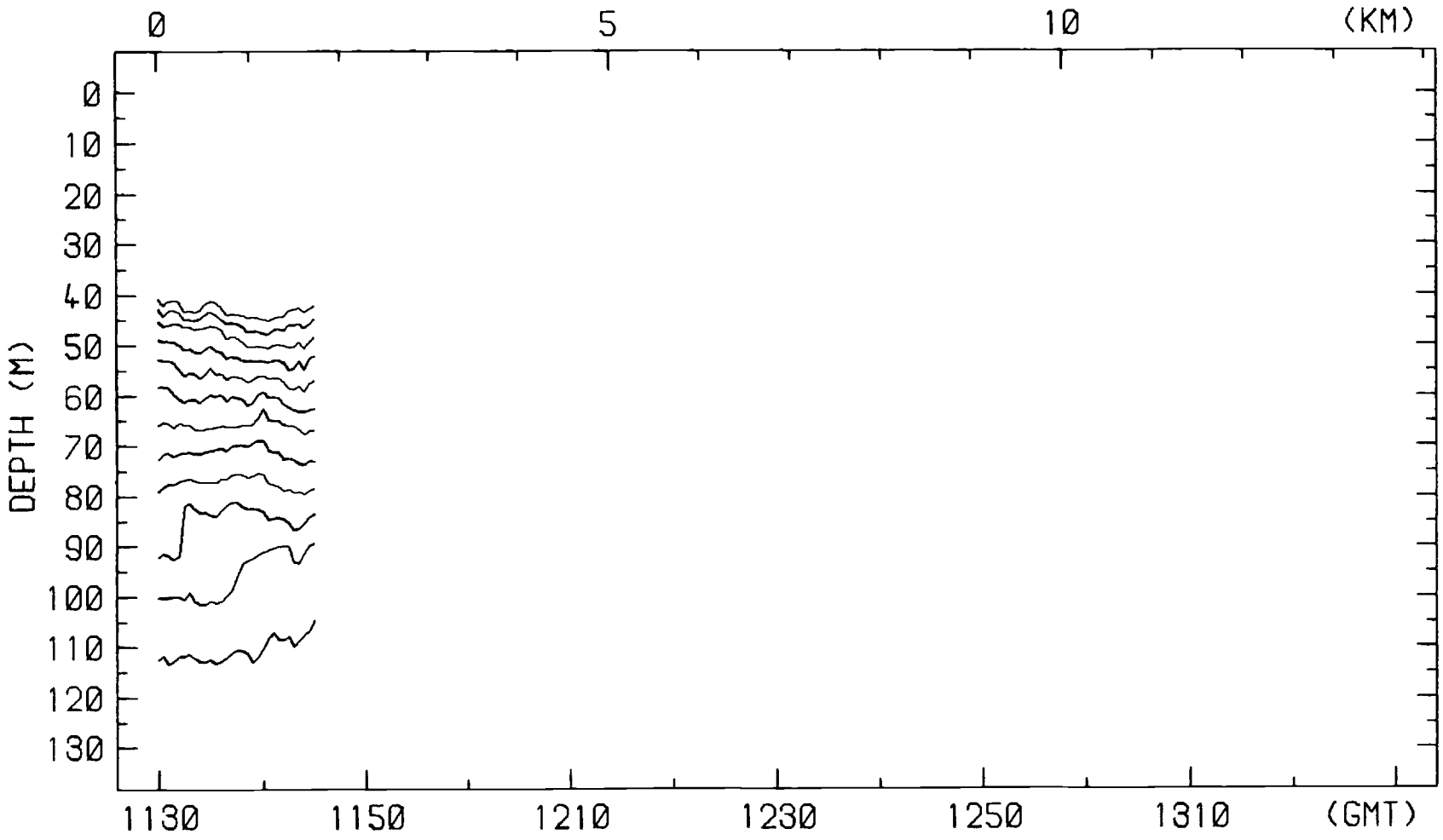

EDITED ISOTHERM DEPTH VS TIME/DISTANCE 14-SEP-81
ISOTHERMS 25.5 TO 20.0 DEG C

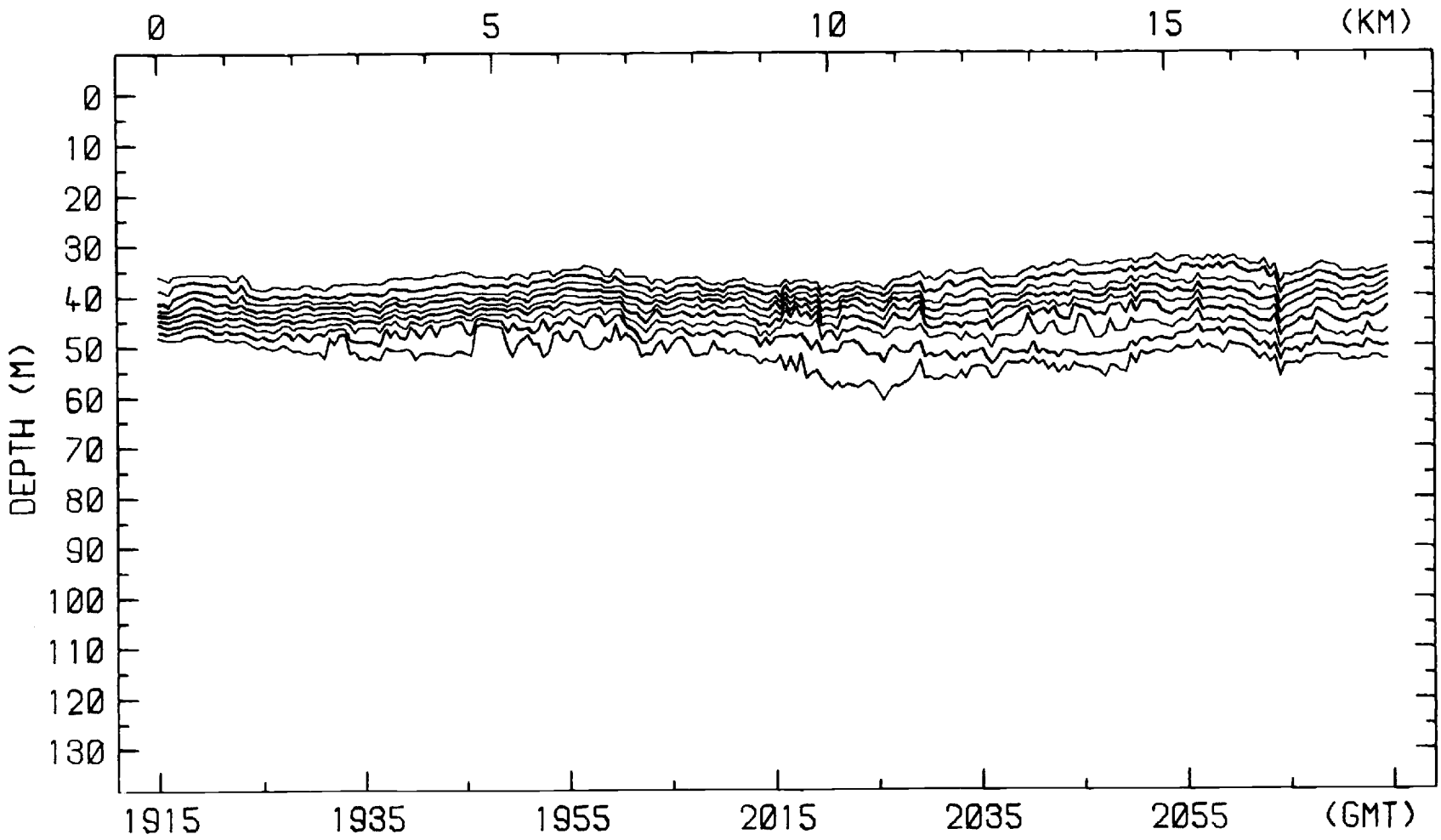

ISOTHERM DEPTH VS TIME/DISTANCE 17-SEP-81
ISOTHERMS 22.0 TO 18.0 DEG C

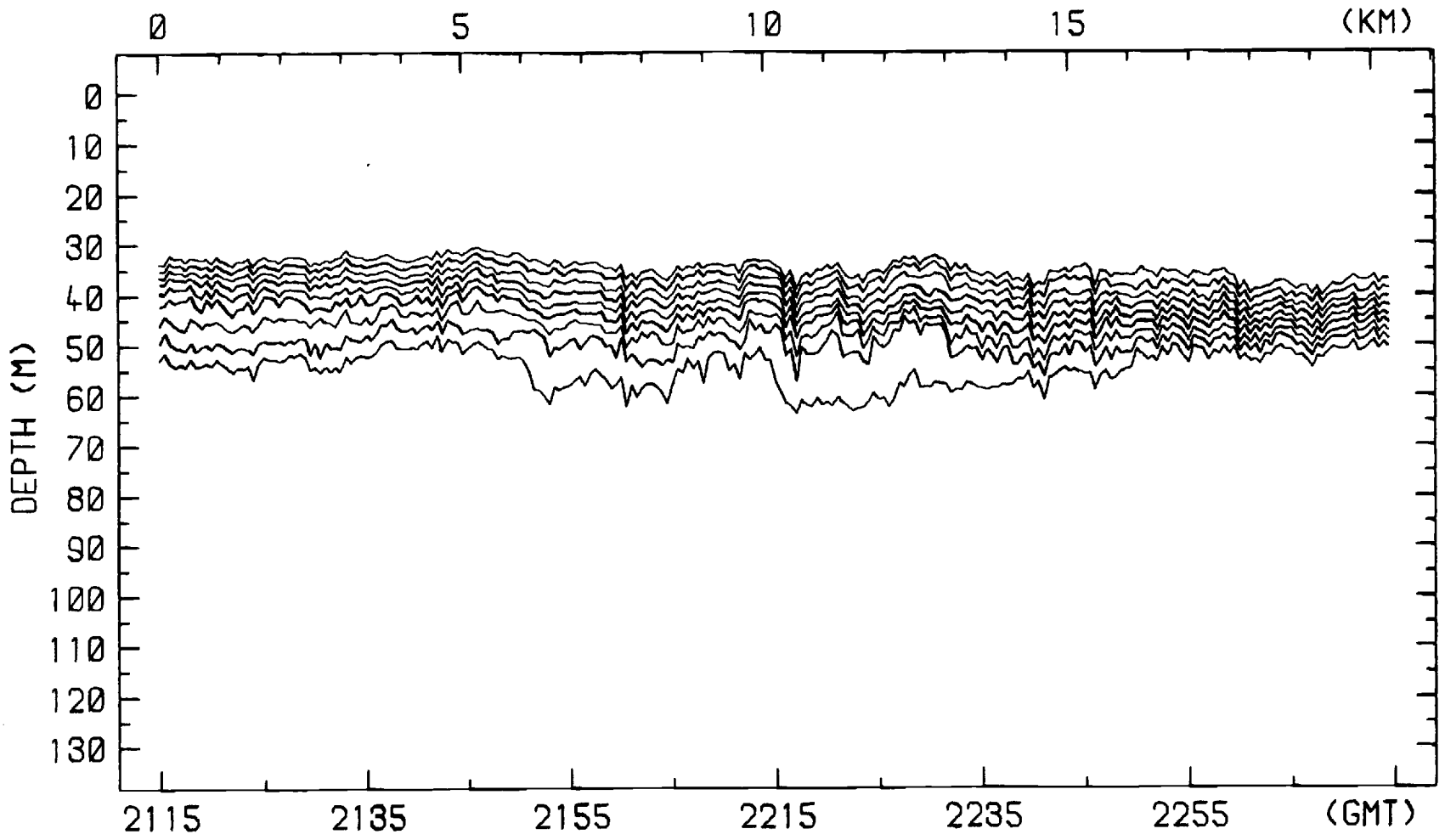

ISOTHERM DEPTH VS TIME/DISTANCE 17-SEP-81
ISOTHERMS 22.0 TO 10.0 DEG C

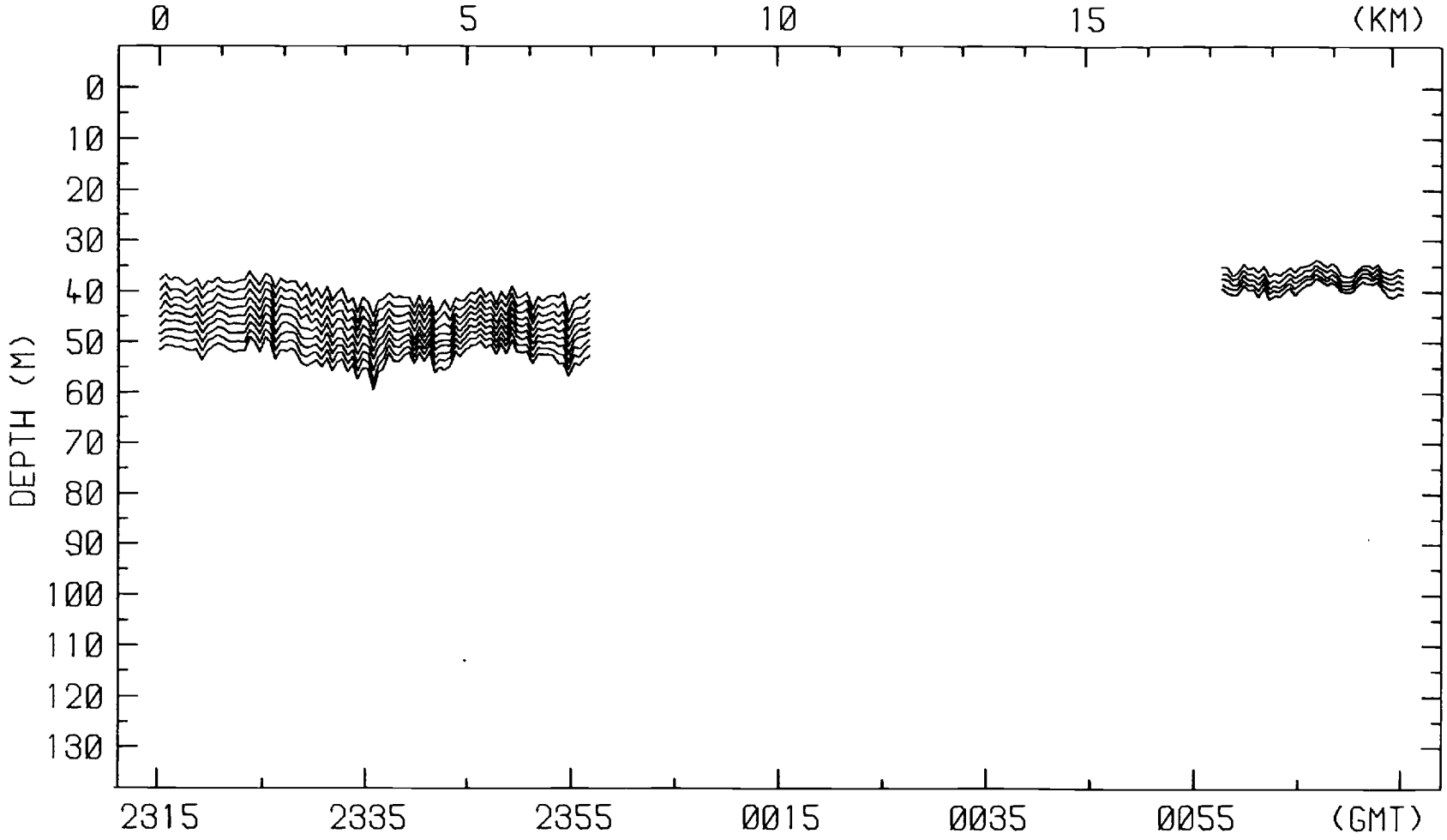

ISOTHERM DEPTH VS TIME/DISTANCE 17,18-SEP-81
ISOTHERMS 20.0 TO 18.0 DEG C

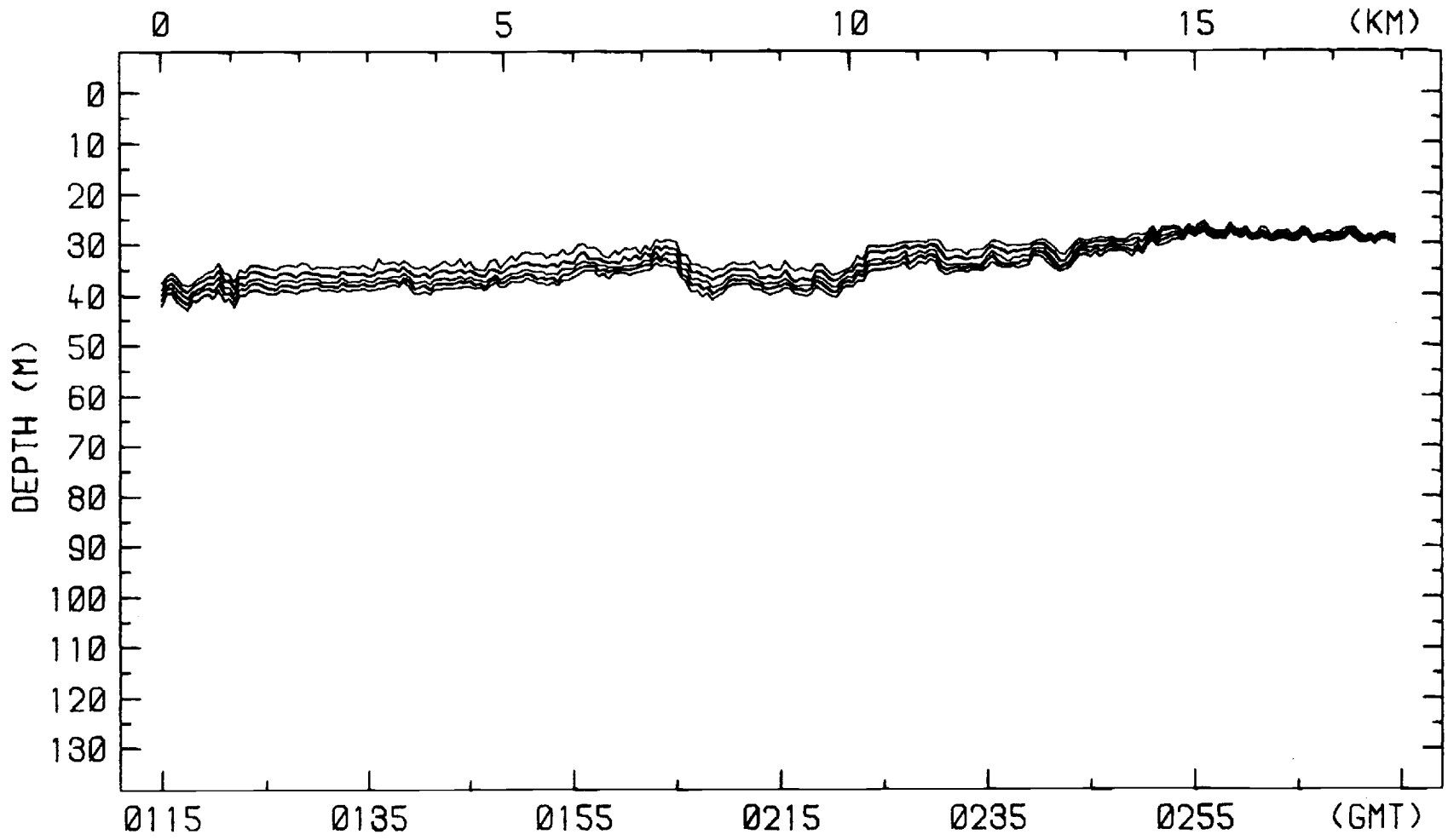

ISOTHERM DEPTH VS TIME/DISTANCE 18-SEP-81
ISOTHERMS 22.0 20.0 DEG C

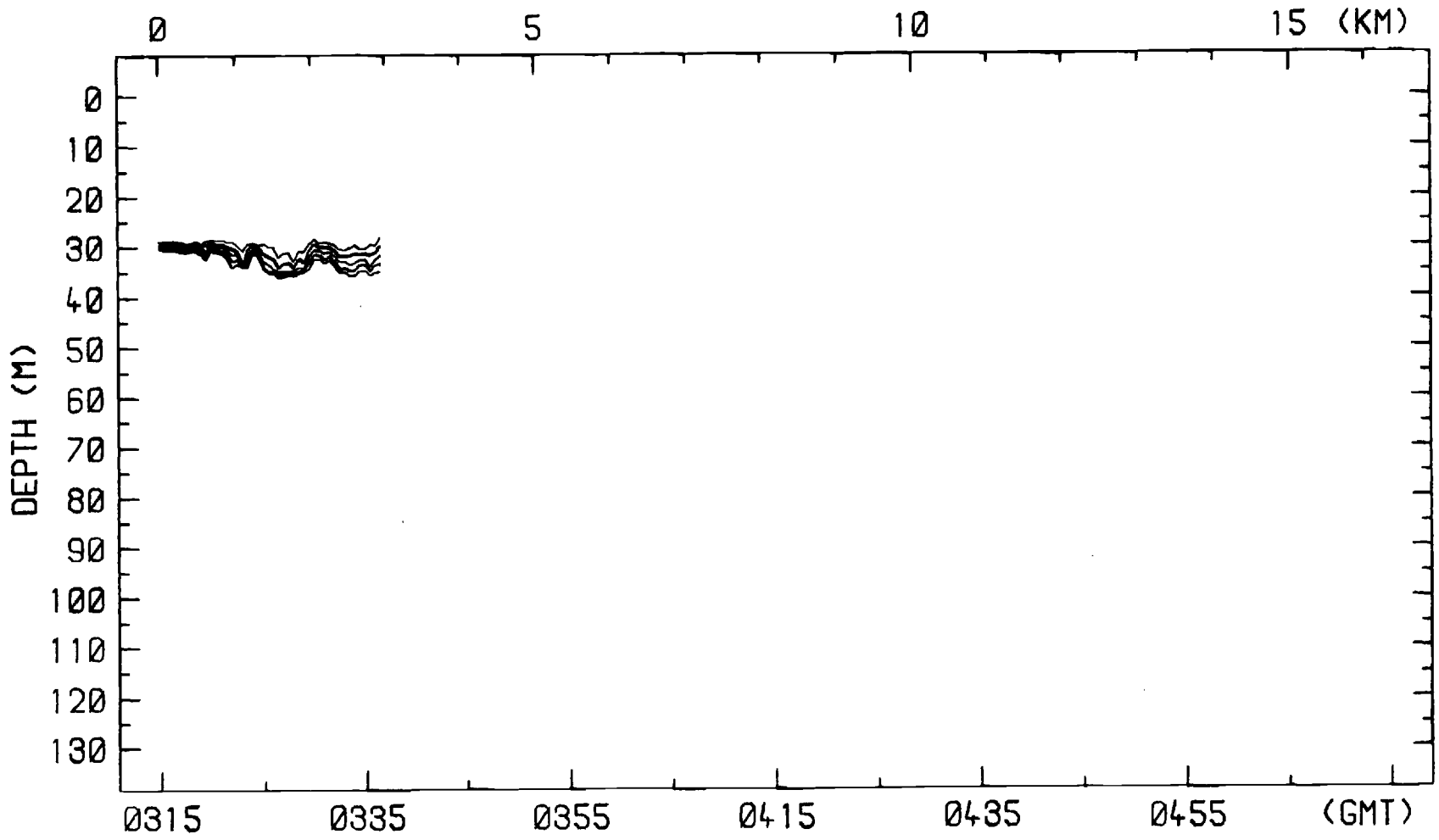

ISOTHERM DEPTH VS TIME/DISTANCE 18-SEP-81
ISOTHERMS 22.0 TO 20.0 DEG C

APPENDIX C

Ensemble Averaged Spectra

This appendix contains the ensemble averaged spectra of Runs 2 and 3 for various depth bands. The spectra were computed by the use of standard techniques. The results of Run 2 are shown before those from Run 3. The run number and depth band of each ensemble average is listed at the top of each figure. A table listing the analyzed isotherms and their average depths is first.

Ensemble Averaged Isotherms

Run 2 14-Sep-81

Depth Band	Isotherm (Deg C)	Average Depth (m)
45-50m	25.5 Tape 9	45.60
	25.0 "	49.40
	25.5 Tape 10	48.00
51-55m	24.5 Tape 9	54.10
	25.0 Tape 10	51.50
	24.5 "	54.70
56-62m	24.0 Tape 9	58.95
	24.0 Tape 10	57.95
	23.5 "	61.50
64-66m	23.5 Tape 9	64.25
	23.0 Tape 10	65.37
70-71m	23.0 Tape 9	70.00
	22.5 Tape 10	70.10
76-77m	22.5 Tape 9	76.60
	22.0 Tape 10	76.15
83-85m	22.0 Tape 9	84.30
	21.5 Tape 10	83.10
90-94m	21.5 Tape 9	93.80
	21.0 Tape 10	90.80
99-105m	21.0 Tape 9	104.90
	20.5 Tape 10	99.70

Run 3 17,18-Sep-81

Depth Band	Isotherm (Deg C)	Average Depth (m)
31-35m	20.5 Tape 13	34.96
	21.0 "	34.09
	21.5 "	33.07
	22.0 "	31.82
35-40m	21.0 Tape 12	39.73
	21.5 "	37.97
	22.0 "	36.17
	20.0 Tape 13	35.76
41-47m	19.0 Tape 12	46.88
	19.5 "	44.77
	20.0 "	43.00
	20.5 "	41.36
49-54m	18.0 Tape 12	53.27
	18.5 "	49.51

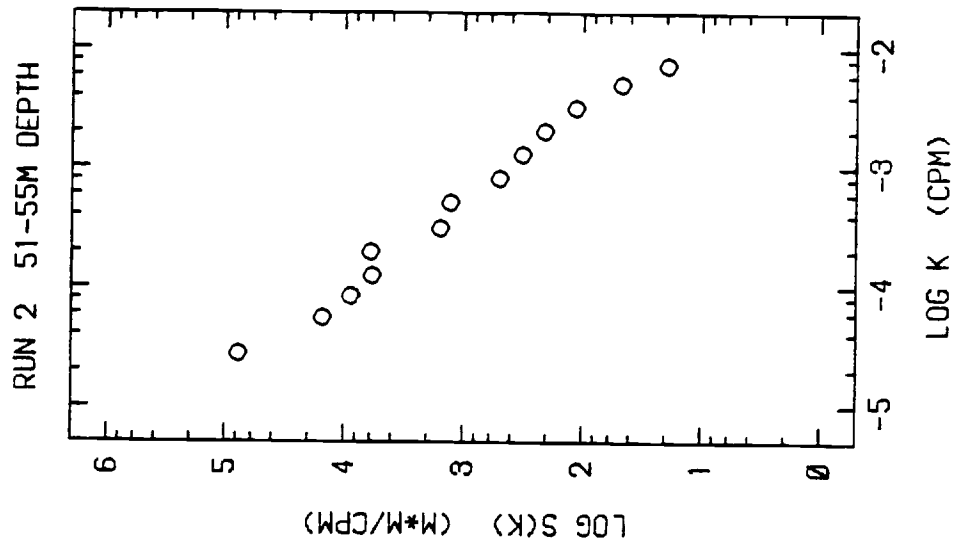
RUN 2 51-55M DEPTH
LOG S(K) (M*M/CPM)
LOG K (CPM)
6
5
4
3
2
1
0
-5
-4
-3
-2

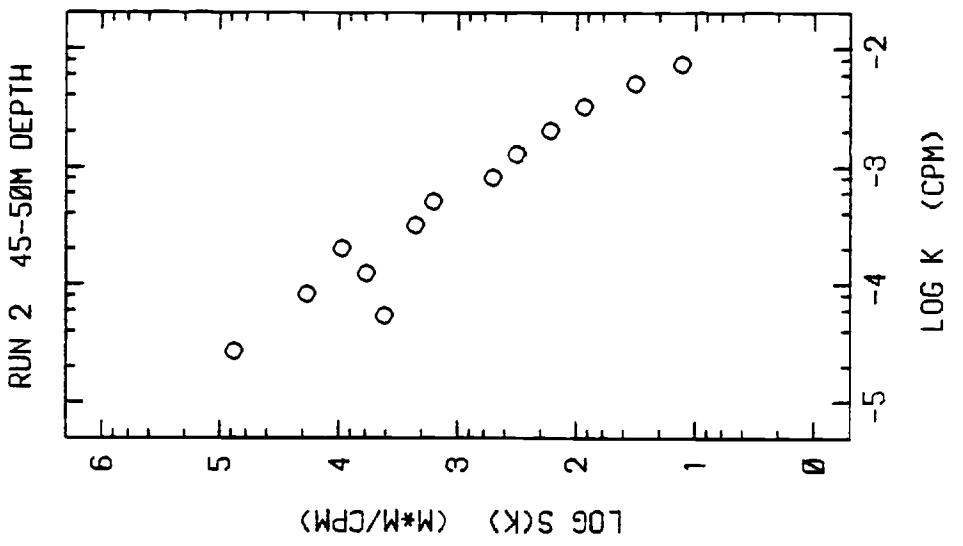
RUN 2 45-50M DEPTH
LOG S(K) (M*M/CPM)
LOG K (CPM)
6
5
4
3
2
1
0
-5
-4
-3
-2

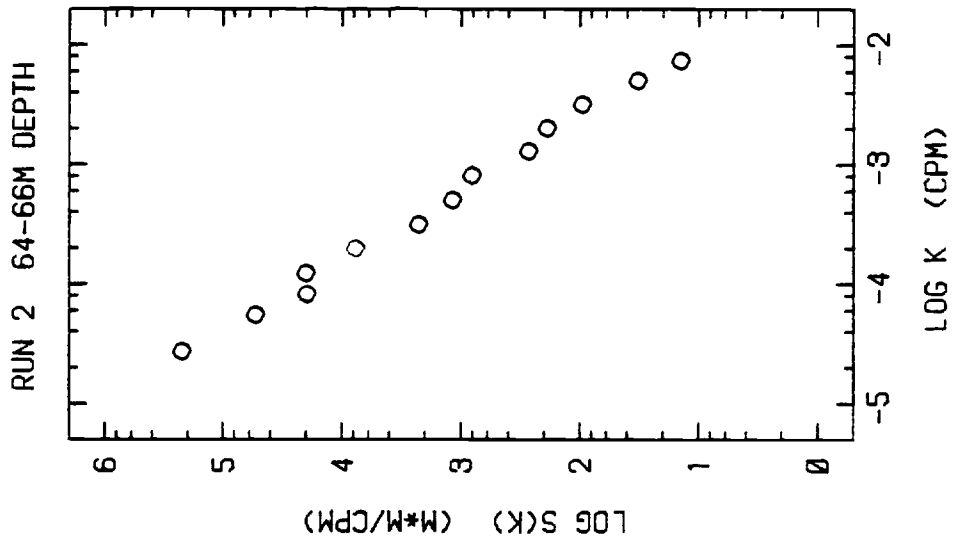
RUN 2 64-66M DEPTH
LOG S(K) (M*M/CPM)
LOG K (CPM)
6
5
4
3
2
1
0
-5
-4
-3
-2

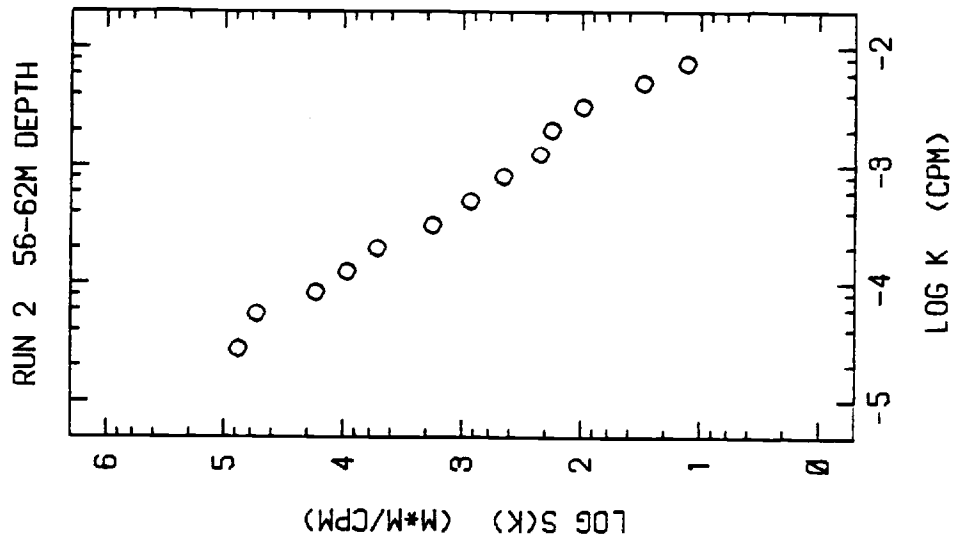
RUN 2 56-62M DEPTH
LOG S(K) (M*M/CPM)
LOG K (CPM)
6
5
4
3
2
1
0
-5
-4
-3
-2

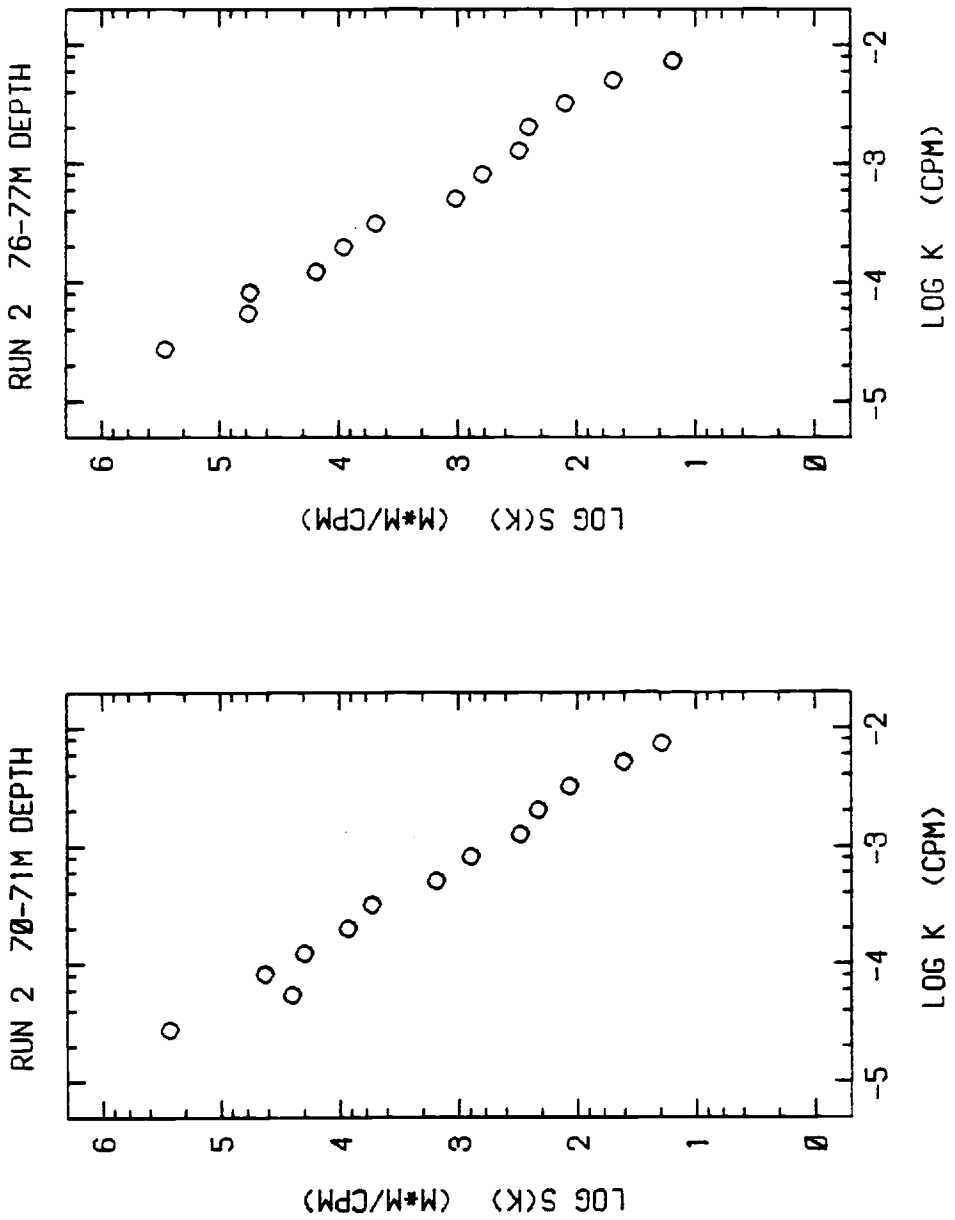
RUN 2 76-77M DEPTH
LOG S(K) (M*M/CPM)
LOG K (CPM)
RUN 2 70-71M DEPTH
LOG S(K) (M*M/CPM)
LOG K (CPM)

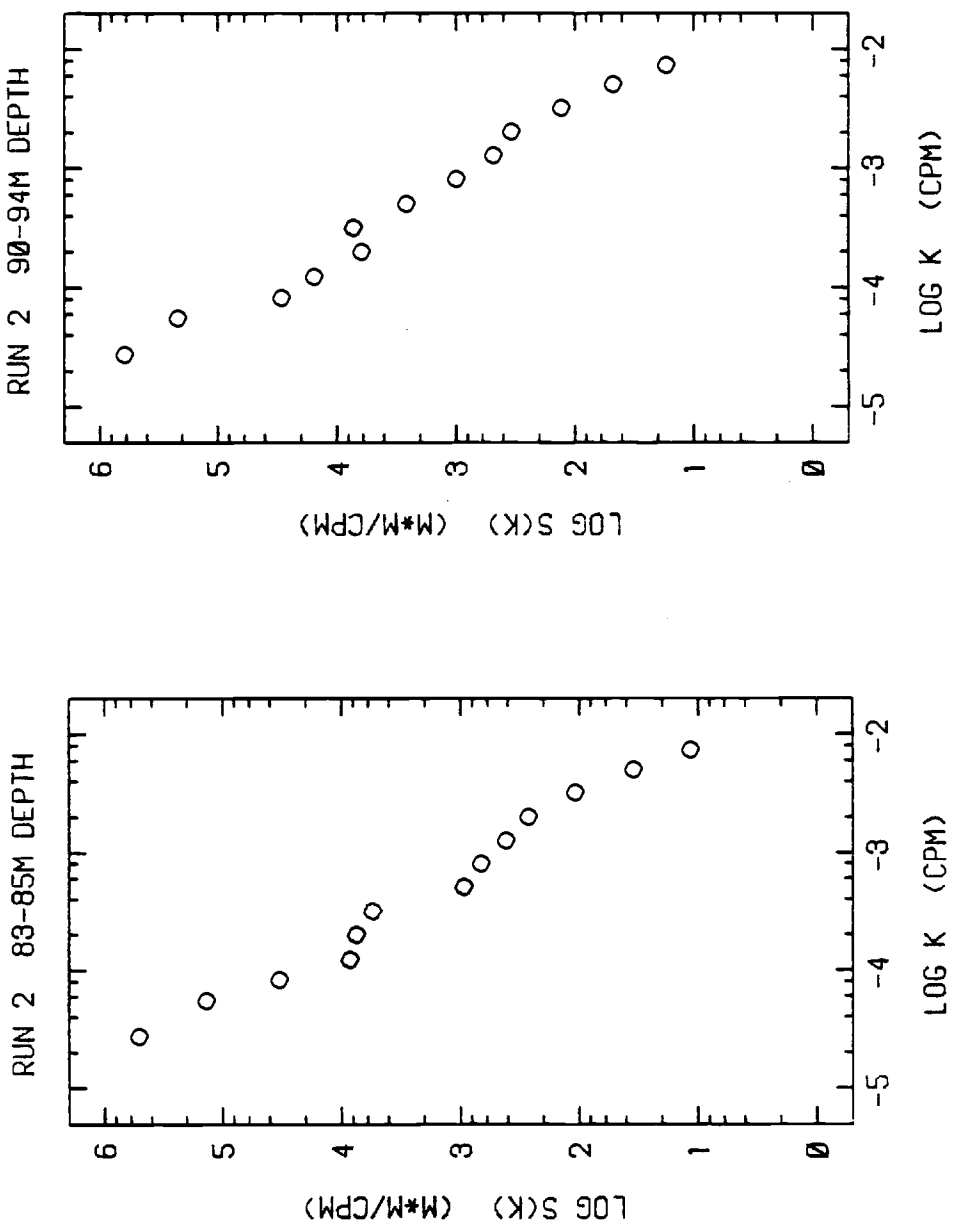
RUN 2 90-94M DEPTH
LOG S(K) (M*M/CPM)
LOG K (CPM)
RUN 2 83-85M DEPTH
LOG S(K) (M*M/CPM)
LOG K (CPM)

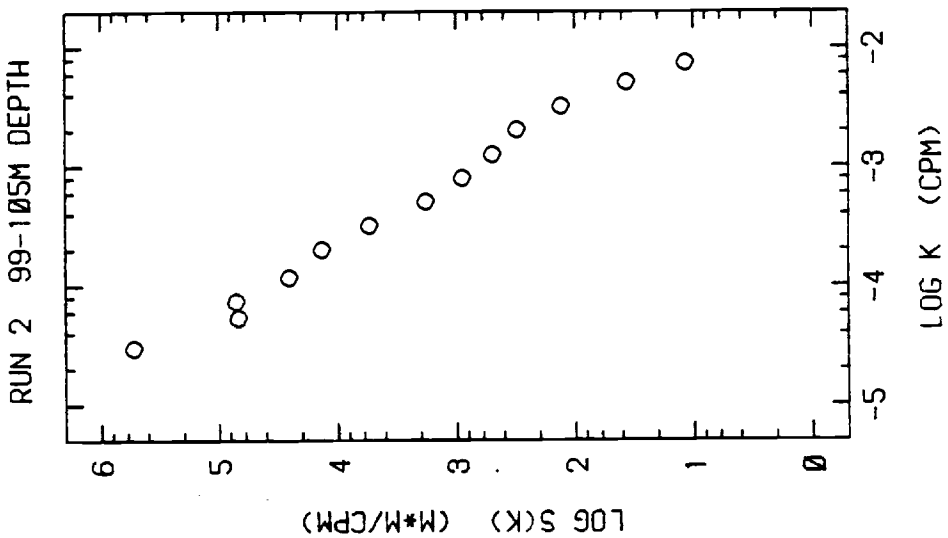
RUN 2 99-105M DEPTH
LOG S(K) (M*M/CPM)
LOG K (CPM)
6
5
4
3
2
1
0
-5
-4
-3
-2

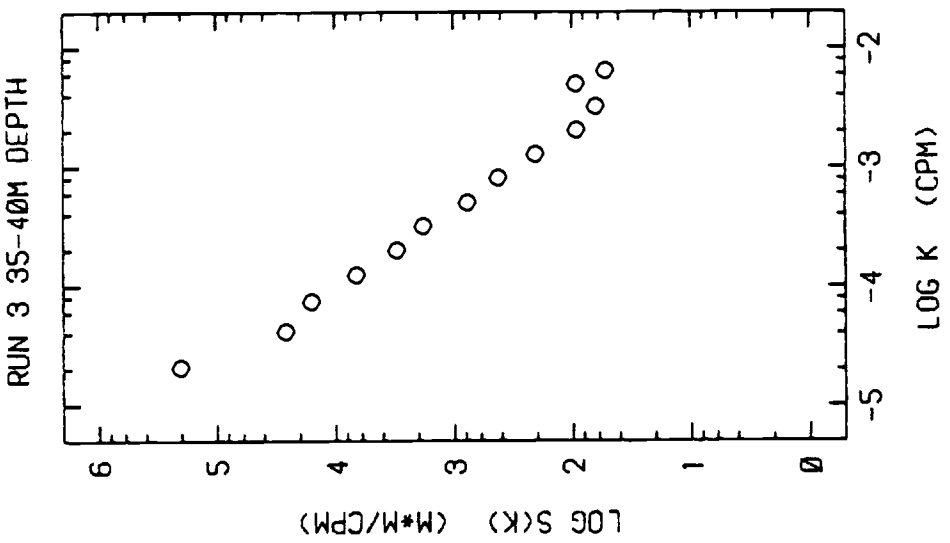
RUN 3 35-40M DEPTH
LOG S(K) (M*M/CPM)
LOG K (CPM)
6
5
4
3
2
1
0
-5
-4
-3
-2

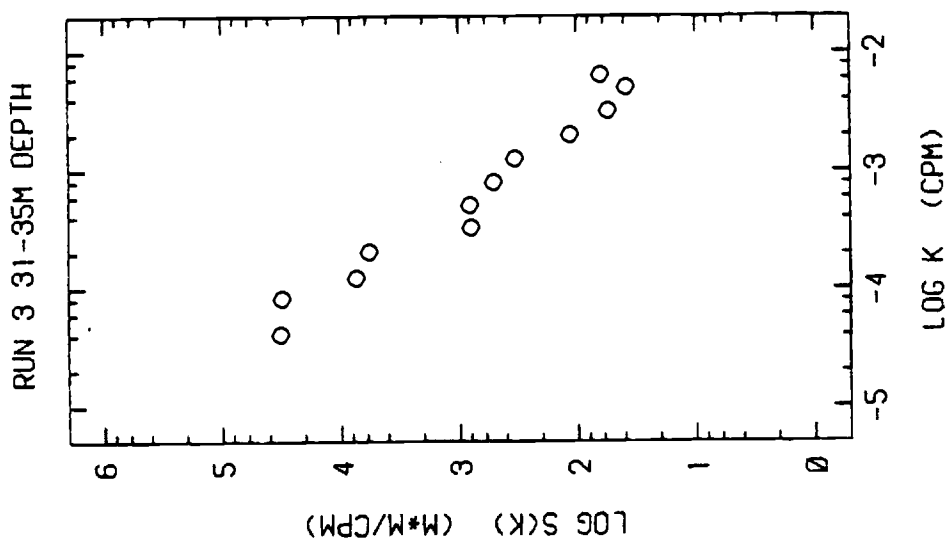
RUN 3 31-35M DEPTH
LOG S(K) (M*M/CPM)
LOG K (CPM)
6
5
4
3
2
1
0
-5
-4
-3
-2

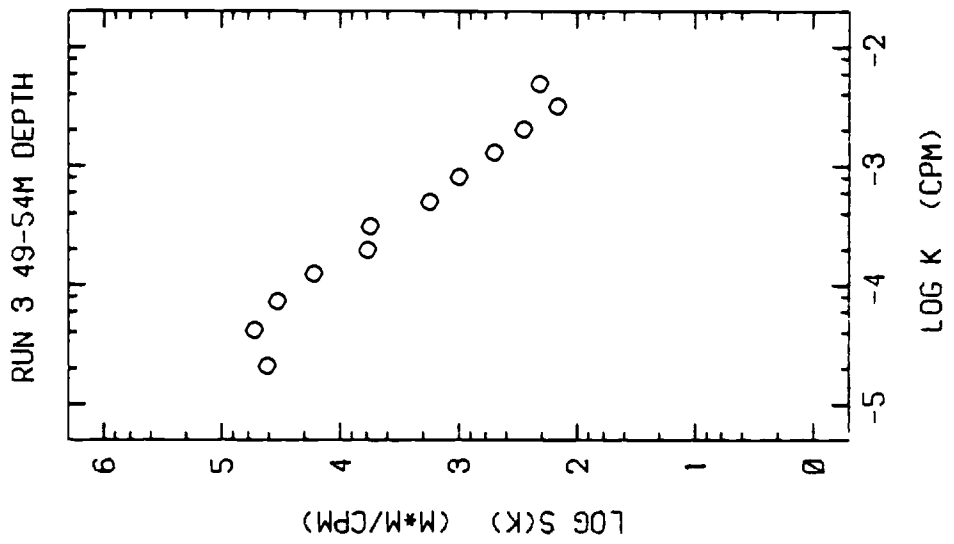
RUN 3 49-54M DEPTH
LOG S(K) (M*M/CPM)
LOG K (CPM)
6
5
4
3
2
1
0
-5
-4
-3
-2

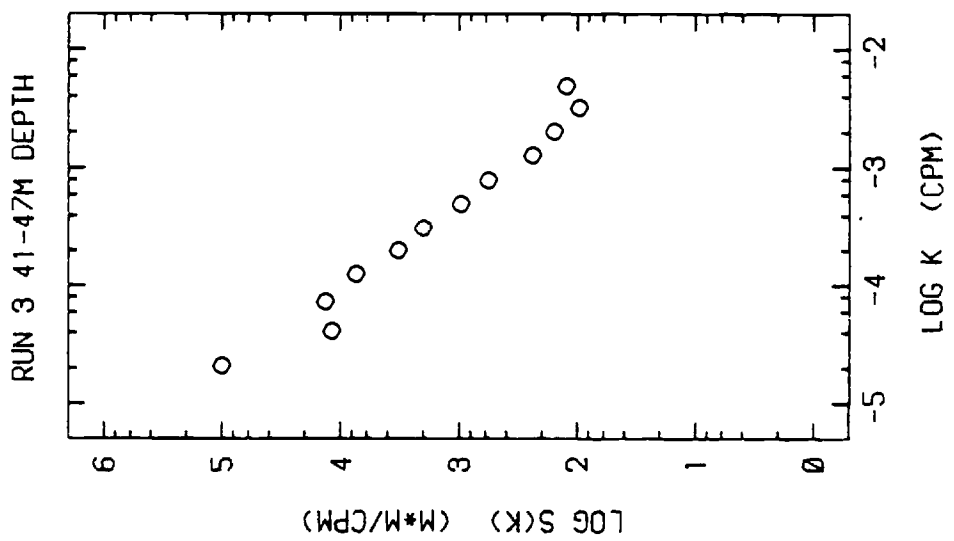
RUN 3 41-47M DEPTH
LOG S(K) (M*M/CPM)
LOG K (CPM)
6
5
4
3
2
1
0
-5
-4
-3
-2

APPENDIX D

Towed Vertical Coherence

The towed vertical coherence as given by Desaubies (1976) is:

$$TVC(2\pi\alpha V) = \frac{(2\pi\alpha V)^2}{\left[\ln\frac{N}{f} - \frac{N^2/f^2 - 1}{2N^2/f^2}\right]} \int_{2\pi\alpha V}^{\infty} \{s^2[s^2-(2\pi\alpha V)^2]^{-1}\} I(s)\,ds$$

where

$$I(S) = (N^2/f^2-1)^2 \int_0^{\infty} t\cos(st)\,[(1+t^2)(N^2/f^2+t^2)^2]^{-1}\,dt$$

α = wavenumber
V = vertical separation
N = buoyancy frequency
f = coriolis parameter.

I(s) can be expressed in terms of exponential integral functions as follows. The integrand of I is expressed in terms of partial fractions.

$$\frac{t\cos(st)}{(1+t^2)(N^2/f^2 + t^2)^2} =$$

$$\frac{B\cos(st)}{1 + t^2} + \frac{(Dt + Ft^3)\cos(st)}{(\gamma + t^2)^2}$$

where

$B = (\gamma - 1)^{-2}$

$D = (1 - 2\gamma)(\gamma - 1)^{-2}$

$F = -(\gamma - 1)^{-2}$ and

$\gamma = N^2/f^2$

Hence

$$I(s) = (\gamma-1)^2 \left[\int_0^\infty \frac{B t\cos(st)\ dt}{(1 + t^2)} + \int_0^\infty \frac{(Dt + Ft^3)\cos(st)\ dt}{(\gamma + t^2)^2} \right] .$$

The first integral

$$B\int_0^\infty t\cos(st)(1+t^2)^{-1}\ dt = B[-1/2(e^{-s}E_i(s)+e^{s}E_i(-s))]$$

(from Gradshyteyn and Ryzhik, 1965)

where $E_i(s) = \int_0^\infty e^t/t\ dt$

$E_i(-s) = \int_0^\infty e^t/t\ dt$.

The second integral can be divided into two integrable parts by adding and subtracting $\gamma t(\gamma+t^2)^{-2}$ to the integrand

$$\int_0^\infty (Dt + Ft^3)\cos(st)(\gamma + t^2)^{-2}\ dt =$$

$$(D/F-\gamma)\int_0^\infty t\cos(st)(\gamma + t^2)^{-2}\ dt + \int_0^\infty t\cos(st)(\gamma + t^2)^{-1}\ dt$$

The first part can be integrated by parts to equal

$$(D/F-\gamma)[1/(2\gamma)-s/2\ \int_0^\infty \sin(st)(\gamma + t^2)^{-1}dt]$$

which, from Gradshteyn and Ryzhik (1965) becomes

$$(D/F-\gamma)[1/(2\gamma)-s/2\{1/(2\sqrt{\gamma})(e^{-s\sqrt{\gamma}}E_i(s\sqrt{\gamma}) - e^{s\sqrt{\gamma}}E_i(-s\sqrt{\gamma})\}].$$

The second part can be evaluated directly from Gradshetyn and Ryshik (1965)

$$\int_0^\infty t\cos(st)(\gamma+t^2)^{-1}dt = e^{-s\sqrt{\gamma}}E_i(s\sqrt{\gamma}) + e^{s\sqrt{\gamma}}E_i(-s\sqrt{\gamma}).$$

Therefore, I(s) becomes

$$I(s) = -1/2[e^{-s}E_i(s) + e^{s}E_i(-s)] - (1-\gamma)\gamma^{-1} +$$
$$[(1-\gamma)s(2\sqrt{\gamma})^{-1} - 1]e^{-s\sqrt{\gamma}}E_i(s\sqrt{\gamma}) +$$
$$[(1-\gamma)s(2\sqrt{\gamma})^{-1} + 1]e^{s\sqrt{\gamma}}E_i(-s\sqrt{\gamma}).$$

The function $TVC(2\pi\alpha V)$ is plotted in Fig. D1 for various values of N/f.

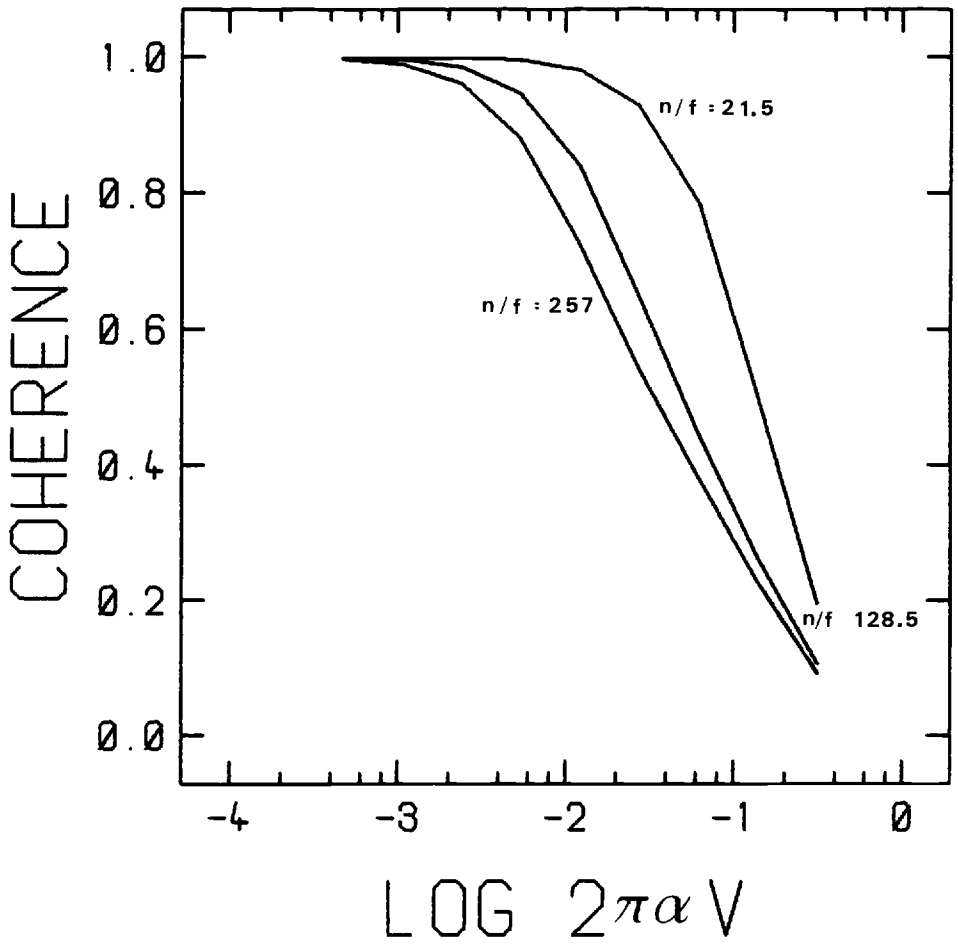

Figure D1. Towed vertical coherence model of Desaubies (1976) at N/f = 21.5, 128.5, and 257. Plotted as coherence vs $2\pi\alpha V$, where α is the wavenumber (cpm) and V is the vertical separation (m).

APPENDIX E

Ensemble Averaged Vertical Coherence

This section contains the ensemble averaged vertical coherences at various vertical separations from Run 2. Vertical coherences from Run 3 were not computed due to the vertical movement of the chain. On each figure, the heavy line is the ensemble average coherence for all isotherm pairs whose vertical separation fit within the the band listed. The table at the beginning of this section contains a list of the isotherm pairs used.

The light line on each figure is the Null Hypothesis test level for each ensemble average. Coherence points which fall below this line cannot be considered significantly different from zero at the 95% level. The dashed line is the model of towed vertical coherence at N = 12 cph as formulated by Desaubies (1976) (see Appendix D).

Vertical Coherence Isotherm Pairs

Separation	Isotherms (Deg C)		Depth Difference (m)
5-10m	23.5-23.0	Tape 9	5.78
	22.0-21.5	"	9.47
	25.5-24.0	Tape 10	9.95
	21.0-20.5	"	8.92
10-15m	25.5-24.0	Tape 9	13.35
	24.5-23.5	"	10.17
	23.0-22.0	"	14.23
	21.5-21.0	"	11.09
	24.5-23.0	Tape 10	10.68
	23.0-22.0	"	10.78
	22.0-21.0	"	14.65
	20.5-20.0	"	10.85
16-20m	24.5-23.0	Tape 9	15.95
	25.5-23.0	Tape 10	17.37
	21.0-20.0	"	19.77
20-25m	25.5-23.0	Tape 9	24.42
	23.5-22.0	"	20.06
	23.0-21.5	"	23.70
	22.0-21.0	"	20.56
	24.5-22.0	Tape 10	21.46
	22.0-20.5	"	22.57
25-30m	23.5-21.5	Tape 9	29.53
	25.5-22.0	Tape 10	28.15
	23.0-21.0	"	25.43
30-35m	24.5-22.0	Tape 9	30.23
	23.0-21.0	"	34.79
	23.0-20.5	Tape 10	34.35
	22.0-20.0	"	34.42
36-40m	25.5-22.0	Tape 9	38.71
	24.5-21.5	"	39.70
	24.5-21.0	Tape 10	36.11
40-43m	23.5-21.0	Tape 9	40.62
	25.5-21.0	Tape 10	42.80
	24.0-20.5	"	41.71

45-53m	25.5-21.5	Tape 9	48.18
	24.5-21.0	"	50.79
	25.5-20.5	Tape 10	51.72
	24.0-20.0	"	52.62
	23.0-20.0	"	45.20
59-63m	25.5-21.0	Tape 9	59.27
	25.5-20.0	Tape 10	62.57

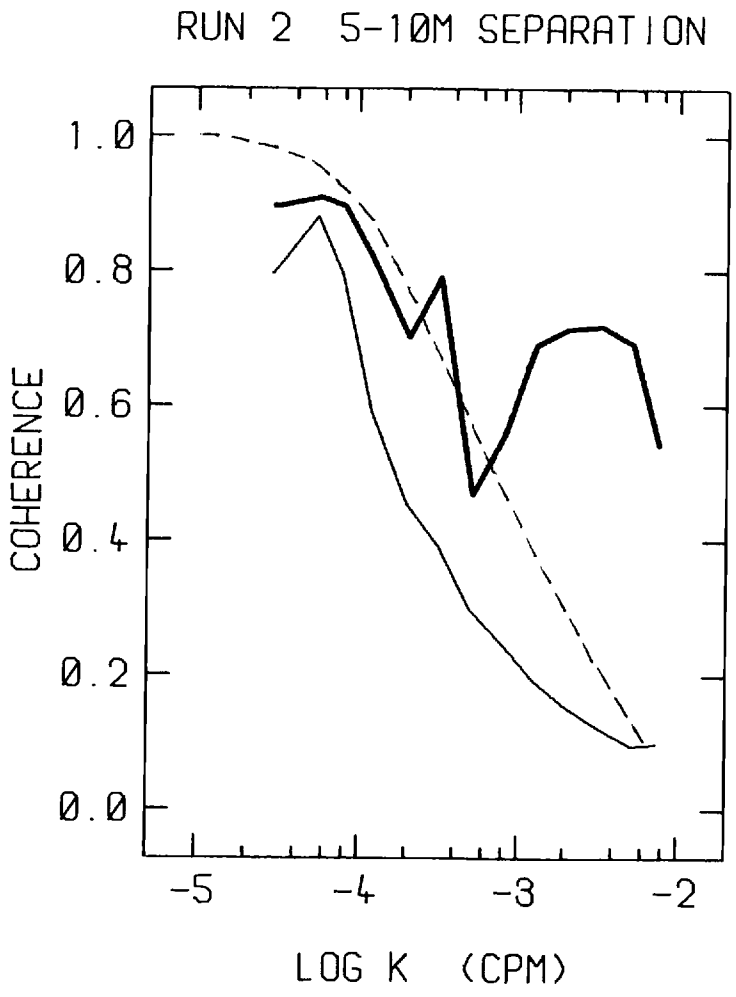
RUN 2 5-10M SEPARATION
COHERENCE
1.0
0.8
0.6
0.4
0.2
0.0
-5
-4
-3
-2
LOG K (CPM)

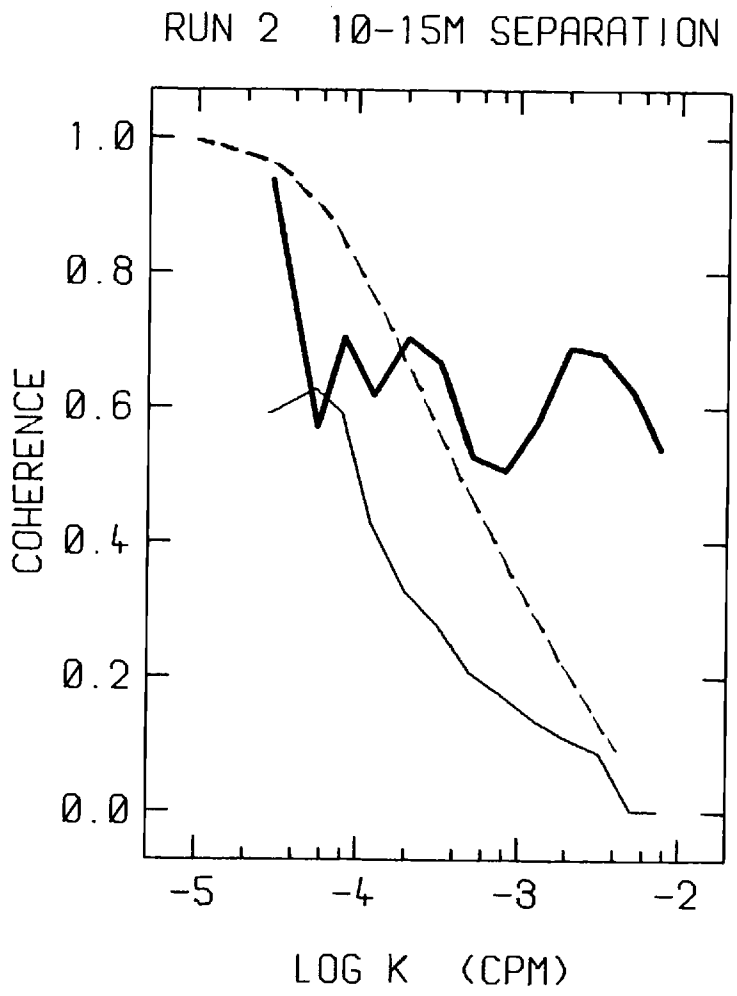
RUN 2 10-15M SEPARATION
COHERENCE
1.0
0.8
0.6
0.4
0.2
0.0
-5
-4
-3
-2
LOG K (CPM)

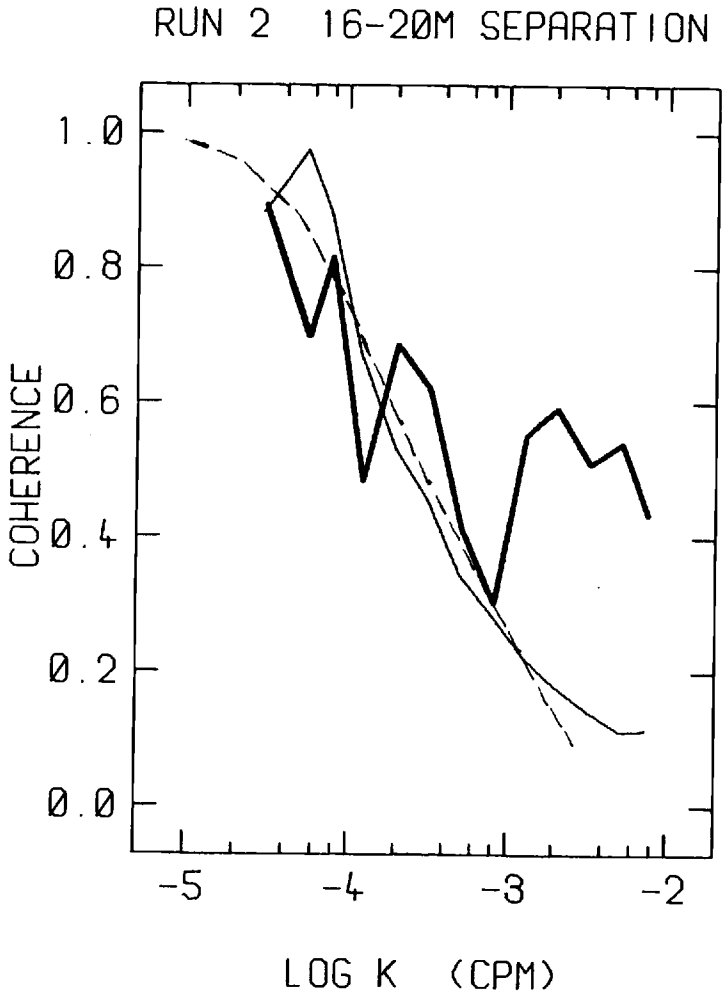
RUN 2 16-20M SEPARATION
COHERENCE
1.0
0.8
0.6
0.4
0.2
0.0
-5
-4
-3
-2
LOG K (CPM)

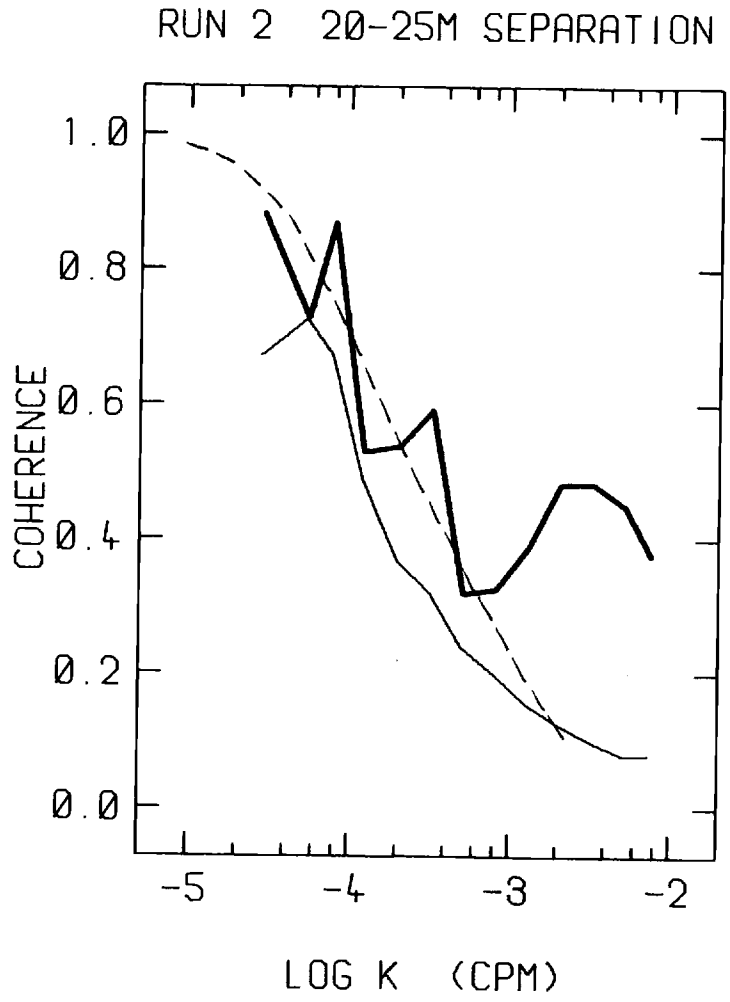
RUN 2 20-25M SEPARATION
COHERENCE
1.0
0.8
0.6
0.4
0.2
0.0
-5
-4
-3
-2
LOG K (CPM)

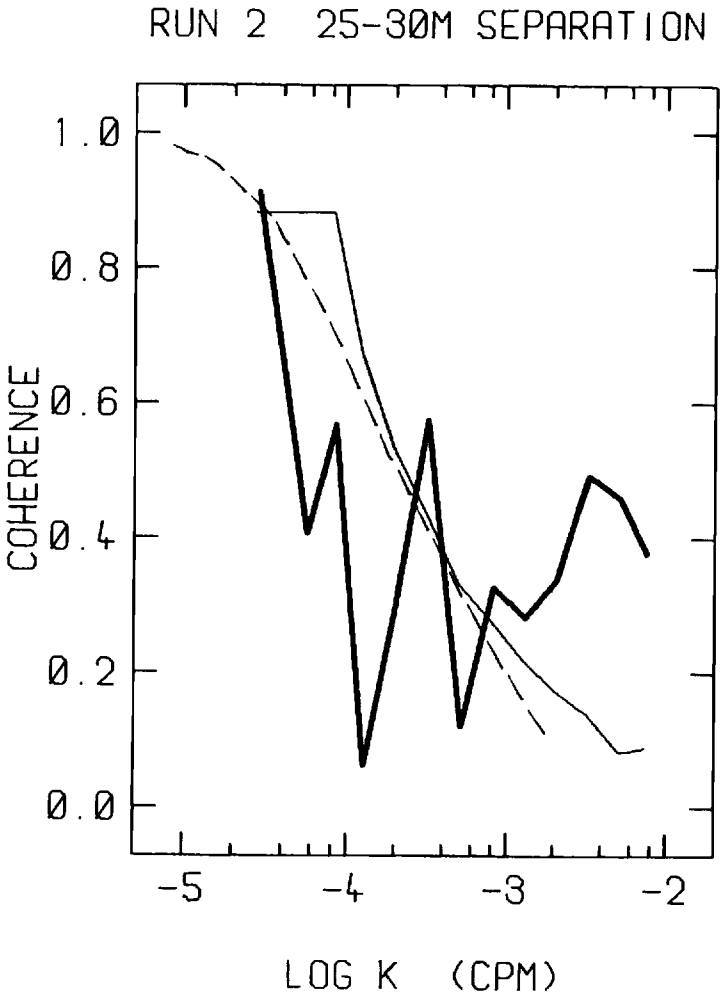
RUN 2 25-30M SEPARATION
COHERENCE
1.0
0.8
0.6
0.4
0.2
0.0
-5
-4
-3
-2
LOG K (CPM)

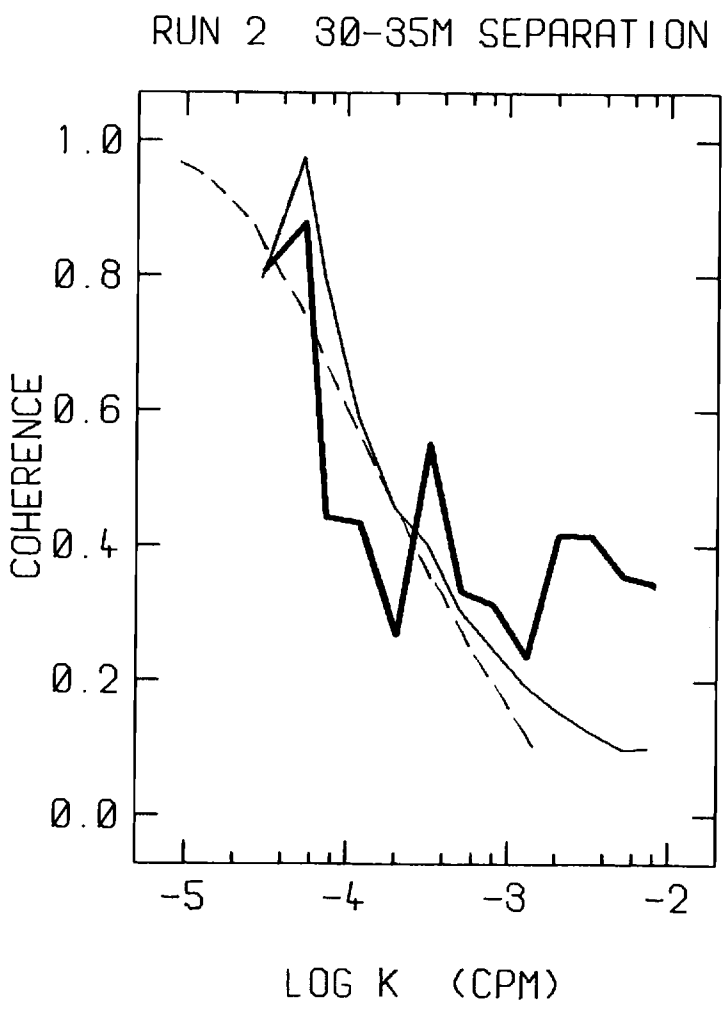
RUN 2 30-35M SEPARATION
COHERENCE
1.0
0.8
0.6
0.4
0.2
0.0
-5
-4
-3
-2
LOG K (CPM)

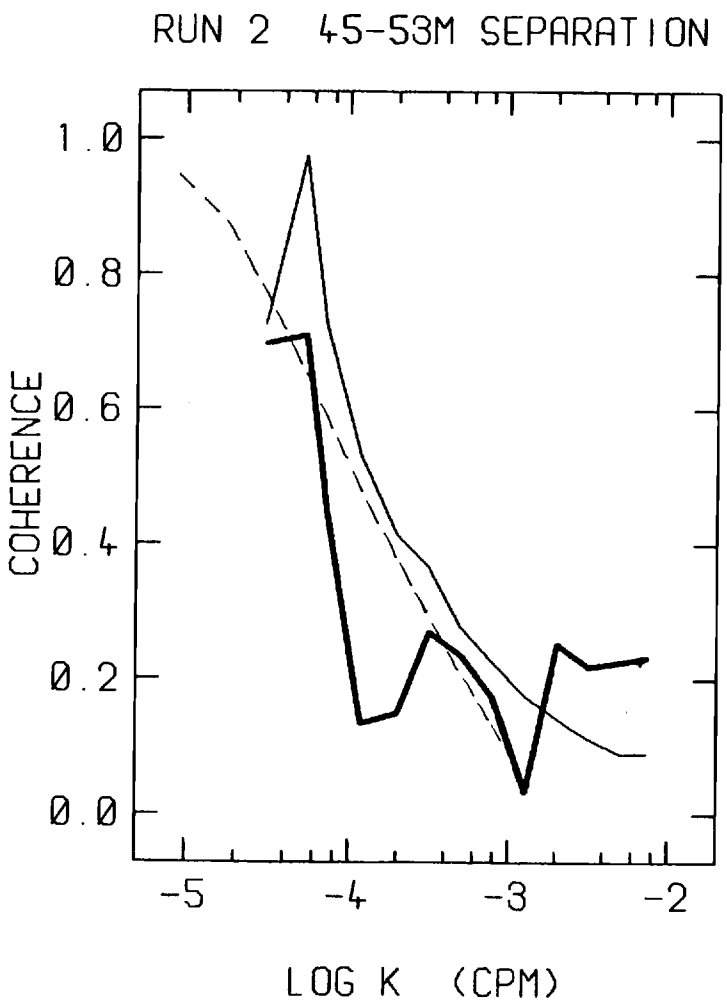
RUN 2 45-53M SEPARATION
COHERENCE
1.0
0.8
0.6
0.4
0.2
0.0
-5
-4
-3
-2
LOG K (CPM)

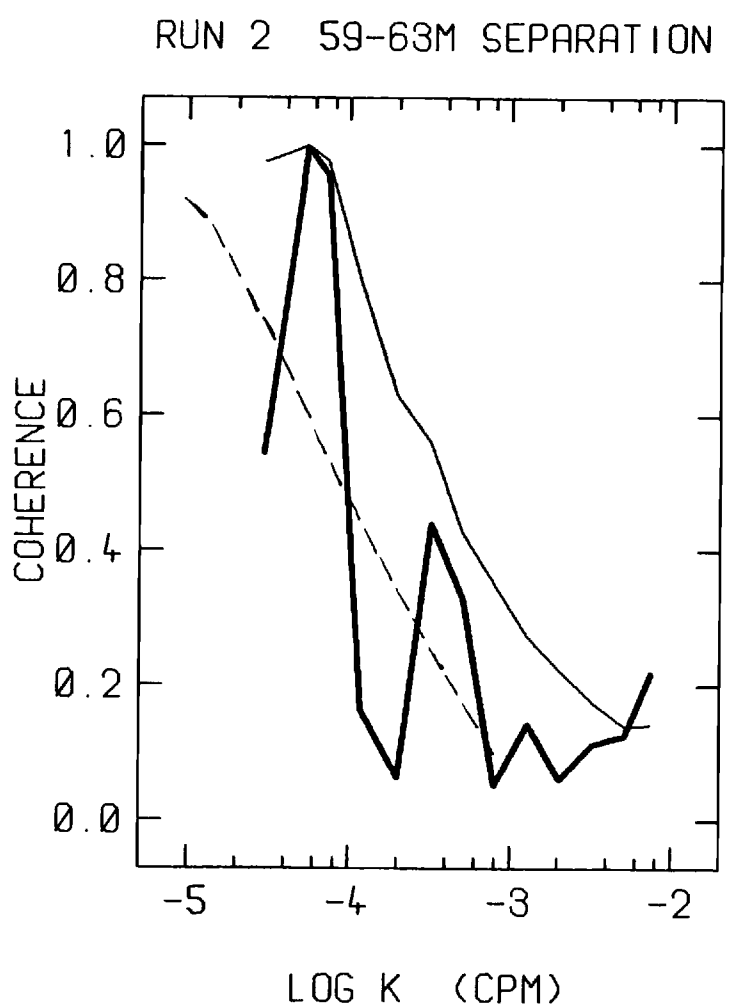
RUN 2 59-63M SEPARATION
COHERENCE
1.0
0.8
0.6
0.4
0.2
0.0
-5
-4
-3
-2
LOG K (CPM)

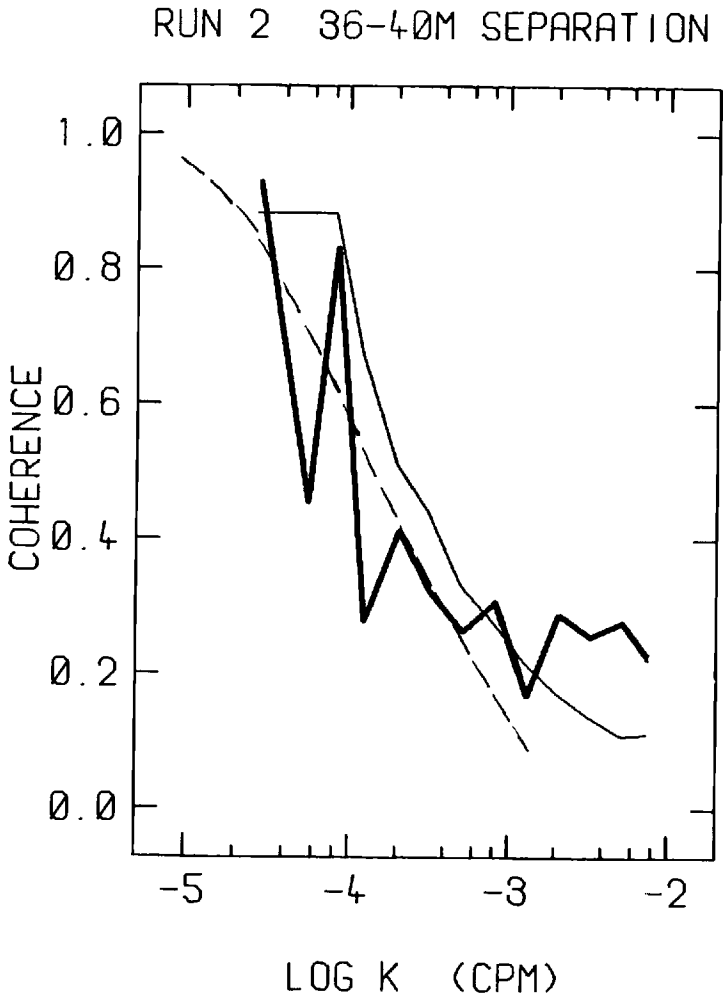
RUN 2 36-40M SEPARATION
COHERENCE
1.0
0.8
0.6
0.4
0.2
0.0
-5
-4
-3
-2
LOG K (CPM)

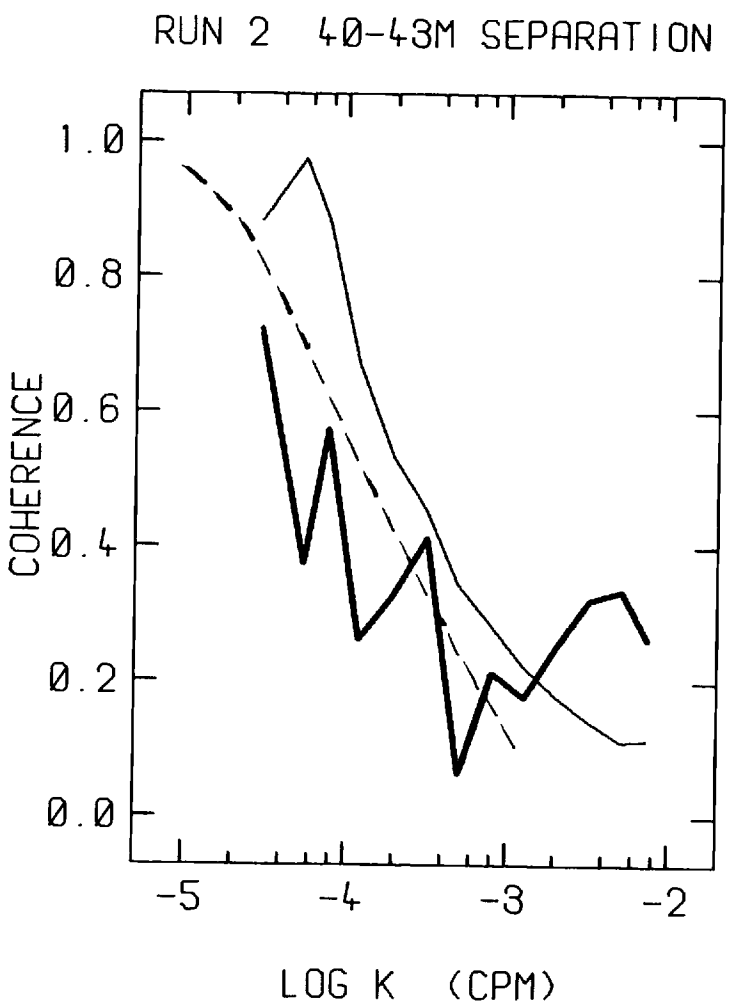
RUN 2 40-43M SEPARATION
COHERENCE
1.0
0.8
0.6
0.4
0.2
0.0
-5
-4
-3
-2
LOG K (CPM)